Modeling of Morphogenesis of Growing Polyolefin Particles

Zdeněk Grof, Juraj Kosek, and Miloš Marek
Dept. of Chemical Engineering, Prague Institute of Chemical Technology, Technická 5, 166 28 Prague 6, Czech Republic

DOI 10.1002/aic.10549
Published online May 10, 2005 in Wiley InterScience (www.interscience.wiley.com).

A novel concept is introduced of modeling of the morphogenesis of polyolefin particles. The polymer particle is assumed to consist of a large number of microelements with binary and ternary viscoelastic interactions acting among individual microelements. These viscoelastic interactions are described by the Maxwell model and govern the morphogenesis process of the growing polymer particle. The rate of the growth of each particular microelement depends on the local catalyst activity and concentration of the monomer. Various types of morphologies of polymer particles are obtained when different viscoelastic properties and/or different reaction conditions are considered. Development of morphological features such as the formation of fine particles, cracks in polymer particles, hollow particles, good or poor replication of the shape of the original catalyst particle, and the evolution of the porous structure of polymer particle are used as illustrative examples. The presented approach thus represents a novel first-principles–based modeling of reaction-transport processes in dynamically evolving multiphase media. © 2005 American Institute of Chemical Engineers *AIChE J,* 51: 2048–2067, 2005
Keywords: polyolefins, morphology, catalytic polymerization, viscoelasticity, porous media

Introduction

Morphology is an industrially important property of polyolefin particles produced in catalytic polymerization reactors. Here we restrict the scope of the notion "morphology" to the shape of particles and to the spatially three-dimensional (3D) distribution of pores, polymer, and catalyst carrier within the particle, respectively. In polymerization reactors, the particle morphology determines the resistance against mass transport of reactants and diluents within the particle and thus it affects the rate of polymerization and molecular architecture of produced polymers.[1] Moreover, it plays an important role in the formation of agglomerates of particles, the sheeting of polymer at reactor walls, and the formation of fine particles in fluidized beds, which are all undesired processes occurring in industrial reactors.[2-4] The control of particle morphology is crucial in the production of micromixed heterophasic materials, such as impact polypropylene.[5,6] In the downstream processing, the particle morphology significantly affects the kinetics of the degassing operation, the mixing of porous particles with additives, and the bulk density and flowability of the powder product.[7]

Despite the importance of the control of morphology, the predictive model describing the process of particle morphogenesis has not been presented yet and our attempt is its development.[8,9] Knowledge in this area is characterized by a number of empirical observations, although a systematic understanding is still missing. Selected experimental observations relevant to the morphogenesis of polyolefin particles are summarized below.

Let us briefly recapitulate the process of particle evolution in gas- and liquid-dispersion reactors for catalytic polymerization of olefins. A typical catalyst of either Ziegler–Natta or metallocene type, supported on the particle of porous catalyst carrier with the diameter 10–50 μm, is injected into a reactor. The polymer starts to fill the pores of the carrier in the early stages of particle growth and the polymer expansion in the confined pore structure of the support causes its fragmentation. Frag-

Correspondence concerning this article should be addressed to J. Kosek at Juraj.Kosek@vscht.cz.

ments of the carrier with immobilized catalyst become encapsulated and are kept together by the polymer. The typical final size of polymer particles leaving the reactor is 0.3–2 mm.

The growth of the polymer particle during catalytic polymerization of olefins has been traditionally described by reaction-transport models with various number of levels of mass- and/or heat-transport resistance and with different constitutive equations describing the transport processes, such as polymer flow model,[10] multigrain model,[11] and dusty fluid model, including the convective transport of reactants.[12] These models impose a number of simplifying assumptions on the geometry of the system and on the description of transport processes: (1) spherical symmetry of the particle, (2) uniform distribution of active catalyst in the growing particle, (3) uniform distribution of micrograins in concentric layers of the particle in the multigrain model,[11] and (4) description of transport processes on the effective (that is, space-averaged) scale. These simplifying assumptions limit the class of addressable problems of particle evolution. The effective-scale descriptions often use the assumption of constant and uniform porosity ε and tortuosity τ applied to the whole particle or to concentric layers of particles in the multigrain model.

Neither the reaction nor the transport processes itself in the model of the growing particle, using spherical symmetry, could describe the evolution of particle structure. A mesoscopic model of particle growth has to: (1) code the spatially 3-D structure of polymer particle, (2) describe the transport processes in the real 3-D pore space, and (3) use first principles for the rules of particle morphogenesis. Moreover, the mesoscopic model has to be computationally feasible. The conceptual ideas and tools required to implement such a mesoscopic model including mechanical properties of porous catalyst carriers and polymer are being developed.[8,9]

The first developed concept makes use of the methodology of reconstructed porous media,[13] where the porous medium is represented by the phase function that can be visualized as the lattice of cubic voxels representing either solid or pore space. The reconstruction of such a pore space from electron microscopy images and the calculation of effective transport properties of the pore structure were demonstrated in our previous work.[14] The reconstructed pore space can also be used to simulate the deposition of catalyst system on a porous carrier and the geometrical prediction of the fragmentation of porous carriers. The disadvantage of the concept of the reconstructed porous medium is that it allows for only small deformations that will not disconnect the semicontinuous solid phase during the particle evolution.

The second concept, elaborated in this work, represents the polymer/catalyst particle as an agglomerate of microelements with force interactions acting among the individual microelements (see Figure 1). Such microelements could be of various types: they can represent the catalyst carrier, active catalyst sites, polymer phase(s), and even the gas occupying the void space. Here we restrict ourselves to one only type of microelement, which is equivalent to the micrograin or to the cluster of micrograins in the multigrain morphology of polyolefin particles.[15] However, morphologies different from the well-developed multigrain structure could also be represented by our model.

The development of such a model faces the problem of a large parametric space and certain ambiguity in the selection of

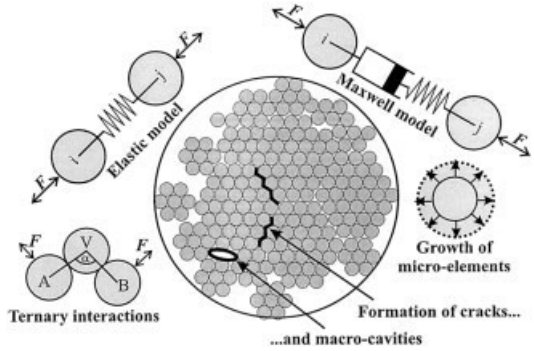

Figure 1. Scheme of the morphogenesis model of polymer particle based on the agglomerate of microelements.

Force interactions $\boldsymbol{F}$ among microelements are schematically represented by elastic and Maxwell models.

a suitable description of viscoelastic interactions among individual microelements. The principal factors affecting the morphogenesis are the magnitude of the built-up stress, the relaxation time of the stress, and the parameters describing the uneven growth of microelements. The differences in the growth rates of microelements are caused both by the nonuniform distribution of catalyst in the microelements and by the nonuniform distribution of monomer concentration in the polymer particle, which could be caused by such factors as mass-transport limitations or pore clogging with a produced polymer.

The mechanical characteristics of polymer and catalyst support were also used by Kittilsen et al.[16] in their description of the growth of polyolefin particles. Their model is based on the assumption of spherical symmetry of the particle or cylindrical symmetry of the single pore of the catalyst support. Estenoz and Chiovetta[17] developed a geometrical model empirically correlating the evolution of particle porosity during its growth. However, their model is more concerned with geometrical representation of a spherical particle with radially varying porosity than with the driving forces of particle morphogenesis.

We recognize the critical role that the catalyst fragmentation plays in the early stages of the polymer particle evolution. The detailed study of such phenomena as the pore clogging with polymer, the transport in the evolving 3-D pore phase of catalyst/polymer particle, and the fragmentation of the porous catalyst carrier is the subject of ongoing research in our group. Experimental study of the fragmentation process at very slow polymerization rates was carried out by Pater et al.[18] and Knoke et al.,[19] who stressed the importance of the rate of polymer formation inside the pores of the support.

This article is organized as follows: First, selected experimental observations of the morphology of polyolefin particles relevant to model formulation are briefly reviewed. Then the physical and mathematical model of the morphogenesis is developed and its simplified version is subjected to theoretical analysis. Finally, numerical simulations with the complete model are shown to reproduce both qualitatively and semiquantitatively the industrially important phenomena such as the formation of fine particles, large cavities in polymer particles, and good or poor replication of the particle shape during its growth. In this article[20] we systematically explore the parametric space of the morphogenesis model for various types of

morphologies and quantitatively compare the predictions of our model with experimental findings available in the literature.

Experimental Observations of Particle Morphology

Particle morphology has traditionally been characterized by the bulk density of the polymer powder, by the distribution of particle sizes and shapes, and by the average intraparticle porosity. More detailed information about particle morphology has been achieved by either transmission or scanning electron microscopy[15,21] and by the application of the high-resolution synchrotron-computed microtomography.[22]

We shall differentiate between the particle morphology and the texture of particle surface observed either by optical or electron microscopy because it is difficult to judge the internal morphology of particles from the texture of their surfaces. The irregular particle shape often manifests itself in the reduced bulk density of the produced powder. However, the bulk density also depends on the particle size distribution, on the porosity of particles, and on the density of the produced polymer. The polymer powder leaving the reactor could remain in storage silos at temperatures around 80°C for many days and this storage increases the bulk density of the powder.[7] The compaction and agglomeration of polymer powder takes place during such a long-term storage because the finer particles fill the interstices between the larger particles and plastic deformation of particles results in the increase of the contact area between the particles. Polymer powders having irregular, spongy particles form stronger compacts than those consisting of spherical and dense particles. The fibrous (wormlike) morphology of some high-density polyethylene (HDPE) powders thus aids in the compaction.[23]

The results of mercury intrusion porosimetry applied to dried polymer samples[24,25] have to be interpreted cautiously because of the effect of the bottlenecking pores, the implicit assumption of cylindrical pores, the uncertainty in the mercury–polymer contact angle, and because of the deformation and the compression of porous polymer material at higher applied pressures.

The multigrain concept of the morphology of polyolefin particles is widely accepted and is well illustrated by electron microscopy images.[15,21] According to this concept, the polymer particle is generally porous and consists of firmly bound structures called *micrograins*, each of which contains a fragment of catalyst inside. However, micrograins are hardly distinguishable in a number of industrial products.

This article demonstrates the capabilities of the model introduced below by addressing the following experimentally observed morphogenesis phenomena:

(1) *Replication of particle shape*. The final shape of polyolefin particles conforms to the initial shape of catalyst particles for a broad range of experimental conditions.[26,27] However, the fast growth of polymer could prevent the regular replication of the shape and the distribution of particle sizes.[28-30] Czaja and Król[31] reported that the non-pre-polymerized $MgCl_2$-supported Ti catalyst produced irregularly shaped polypropylene particles, whereas the prepolymerized catalyst particles yielded oval particles with a nearly uniform distribution of shape and size.

(2) *Formation of macrocavities in particles*. The porous space is not homogeneously distributed on the scale of the polymer particle. Investigations of sections of polyolefin particles by electron microscopy revealed in many cases the existence of cavities with a characteristic size $\gtrsim 5\ \mu$m.[22,27] Also the sections of embedded particles in the studies conducted by both Debling and Ray[5] and Kittilsen and McKenna[32] revealed the presence of large pores, holes, or channels deep within both the homopolymer and copolymer particles. These large pores separate the areas having lower porosity and significantly affect the transport in the polymer particle. The potential origins of observed macrocavities are numerous, such as a replication of the inhomogeneous structure of catalyst particle, mass-transport limitations in the growing particle resulting in the nonuniform concentration field within the particle, the clogging of particle pores by polymer, and a nonuniform distribution of catalyst in micrograins. The morphogenesis model proposed herein could help to discriminate between them.

(3) *Formation of hollow particles*. Impregnation of the surface layer only of the porous catalyst carrier by the catalyst could result in the formation of hollow polymer particles in the reactor. A similar effect could also be observed as the consequence of severe mass-transfer limitations in the polymer particle as observed by Debling and Ray.[5] They found in their comprehensive study on the evolution of the morphology of impact polypropylene that the particle with 70 wt% of soft ethylene–propylene rubber was hollow, suggesting that the pores near the outer layers of the particle were choked with a soft copolymer.

(4) *Formation of fine particles*. Here we demonstrate the mechanism of the formation of fine particles by mechanical disintegration of the vigorously growing catalyst/polymer particles within a certain range of reactor conditions in accordance with the observations made by Llinas and Selo.[2] However, a number of other causes related to this industrially important problem could be formulated, such as the deactivation of catalyst particles in the early stage of their growth and the breakage of particles during their mutual collisions. The fine particles could be loosely defined (such as particles with the equivalent diameter $< 125\ \mu$m) and their shape is often highly irregular.[23] Although the fraction of fines in the reactor represents a low percentage of total mass, it represents a considerable number of particles that are susceptible to adhere to reactor walls because of their small size. Llinas and Selo[2] suggest that the fines could be the precursor of particle agglomerates.

(5) *Evolution of particle porosity*. The porosity of catalyst carriers is typically >50% and the porosity of final polymer particles is significantly lower.[27] The prediction of final particle porosity by a first-principles model is a challenging task. For example, the porosities of polyolefin particles obtained from the supported metallocenes are often lower than those obtained under the same conditions with traditional Ziegler–Natta catalysts.[33,34] The enhanced incorporation of comonomers into polymer chains by metallocenes is probably an important factor in this respect.

Most of these morphogenesis phenomena were not described by other models of growing polymer particles or were addressed to only a limited extent.

In our model we consider some often overlooked aspects of the multigrain morphology. Submicron-sized micrograins are usually assembled in clusters, within which the submicron pores are apparent, but the larger micron-sized pores separating

the cluster are also present in polymer particles.[5,35] The origin of these clusters of micrograins could be a replication of the microstructure of porous catalyst carriers. One of the commonly used templates of the catalyst carrier is the colloidally precipitated silica that consists of primary nanosized particles aggregated into clusters with characteristic size of tens of nanometers, which are assembled into superclusters with characteristic size of hundreds of nanometers. Another mechanism of the formation of clusters could be the progressive subdivision of catalyst carriers into increasingly smaller fragments, where the smallest fragments represent the centers of tightly bound micrograins. However, the clusters could also be a natural demonstration of the self-organization of the porous structure of polymer particle on the microscale.

It is hardly computationally feasible to consider all individual micrograins in our morphogenesis model of particle evolution, and thus the clusters of micrograins could also be considered as principal building blocks (microelements) of a polyolefin particle.

Debling and Ray[36] proposed a modification of the multigrain model of particle growth[11] by introducing a "compressibility factor" of polymer phase accounting for the deformation of micrograins, thus reducing the particle porosity. This compressibility factor of the micrograin was designed in an empirical geometrical way without a direct link to mechanical properties of the produced polymer. This improvement allowed the multigrain model to slowly decrease the particle porosity with time, in agreement with typical growth of polymer particles at mild reactor temperatures.

Herein we attempt to link semiquantitatively the evolution of particle structure and porosity to mechanical viscoelastic properties of the produced polymer, such as those of isotactic polypropylene, Ziegler–Natta- and the metallocene-supported polyethylene, or various copolymers.

Polymer Particle as an Agglomerate of Microelements

The polymer particle, consisting of both a semicrystalline polymer phase and a carrier with immobilized catalyst and pores, can be discretized into small microelements. The microelements can be of different types, such as the polymer phase and the catalyst carrier microelements, as used in our ongoing work on the fragmentation of porous catalyst supports. The reaction, transport, and mechanical deformation processes are considered to take place in the interconnected network of microelements (see Figure 1). For the sake of simplicity, all microelements have a spherical shape.

Herein we use only one type of microelement that is conceptually equivalent to the micrograin in the multigrain model of growing polymer particle,[36] that is, each microelement consists of the fragment of catalyst carrier with active catalyst sites immobilized on its surface encapsulated in the polymer. However, the microelement could also represent the cluster of micrograins, which tends to behave as a building block of the polymer particle, and thus the equivalence between the micrograin and the microelement is loose. Agglomerates of microelements could well represent particle morphologies other than the multigrain morphology[15,21] because the microelements could partially interpenetrate or the connections among microelements could break.

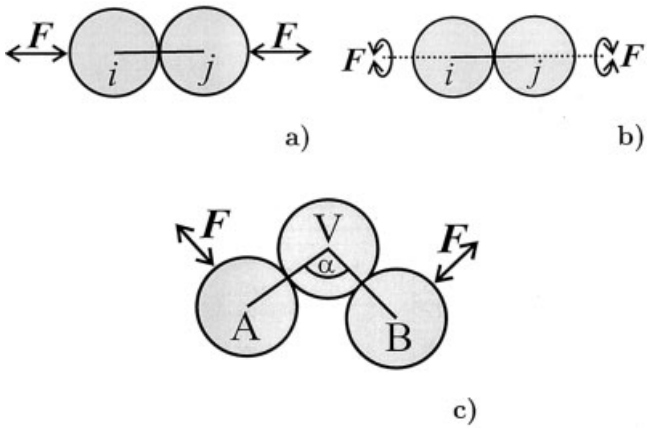

Figure 2. Illustration of force interactions among microelements.

(a) Resistance against "push" and "pull"; (b) resistance against "torsion"; (c) resistance against "change of bonding angle" (that is, ternary interaction).

Mechanical (force) interactions among microelements (see Figure 2) are calculated at each time step of dynamic simulation and the translational movement of microelements is updated according to the Newton's law

$$\frac{d\boldsymbol{x}_i}{dt} = \boldsymbol{v}_i \qquad \frac{d(m_i\boldsymbol{v}_i)}{dt} = \sum_j \boldsymbol{F}_{ij}^{\text{binary}} + \sum_{j,k} \boldsymbol{F}_{ijk}^{\text{ternary}} \tag{1}$$

where t is time and $\boldsymbol{x}_i$, $\boldsymbol{v}_i$, and m_i are position vector of the center, velocity, and mass of the ith microelement, respectively. The summations of forces $\sum \boldsymbol{F}_{ij}$ and $\sum \boldsymbol{F}_{ijk}$ are carried out over all binary and ternary interactions between the ith microelement and its connected neighbors. The rotational movement of microelements displayed in Figure 2b is not considered herein for the sake of simplicity.

The volume of the ith spherical microelement is $V_i = (4/3)\pi r_i^3$ and its mass is $m_i = \rho_i V_i$, where r_i is the radius and ρ_i is the density of the microelement. The evolution of the microelement volume and mass depends on its rate of growth dr_i/dt, as follows

$$\frac{dV_i}{dt} = \frac{3V_i}{r_i}\frac{dr_i}{dt} \qquad \frac{dm_i}{dt} = \frac{3m_i}{r_i}\frac{dr_i}{dt} \tag{2}$$

where the simplification of constant microelement density ρ_i is used throughout this article.

The rate of growth of each particular microelement depends on: (1) the amount of active catalyst sites inside the microelement and (2) the concentration of monomer(s) and other reactants at active catalyst sites (dependent on the concentration of species surrounding the microelement and their transport through the polymer to the active catalyst sites located at the surface of catalyst carrier). The effect of monomer transport through the polymer phase of microelement is neglected in this study.

The rate of growth of the ith microelement is in the simple case of a homopolymerization, described as

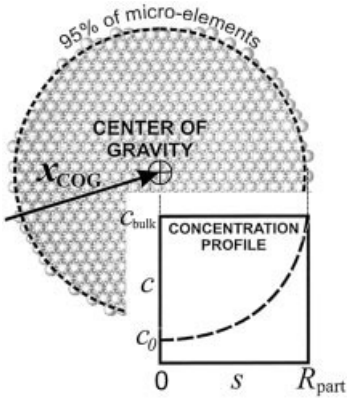

Figure 3. Concentration profile in the agglomerate of microelements.

$$\frac{dm_i}{dt} = km_{\text{cat},i}c_i \tag{3}$$

where $m_{\text{cat},i}$ is the mass of catalyst in the ith microelement and c_i is the concentration of the monomer at the surface of the ith microelement. Let A_Y be the polymer yield rate at reactor bulk temperature in $\text{kg}_{\text{pol}}/(\text{g}_{\text{cat}}\ \text{h})$. Then the reaction rate constant is $k = A_Y/(3.6c_{\text{bulk}})$, where c_{bulk} is the bulk concentration of monomer in the reactor. The generalization of Eq. 3 to the case of copolymerization is obvious. The Arrhenius dependency of rate constant on temperature is considered in the discussion of the influence of temperature on the particle morphogenesis

$$k = k_0\exp[-E_A/(RT)] \tag{4}$$

where k_0 is a preexponential factor, E_A is the activation energy, R is the gas constant, and T is temperature.

The more general case of interpenetrating microelements is treated in the Appendix. The state variables of the model are $\boldsymbol{x}_i$, $\boldsymbol{v}_i$, and r_i, where $i = \{\text{all microelements}\}$. This list of state variables is not complete because the constitutive equations describing force interactions required in Eq. 1 can be differential (see below).

Transport Limitations in Polymer Particles

We consider the effect of nonuniform distribution of monomer concentration c_i on the morphogenesis of a polymer particle consisting of microelements. Although the description and the simulation of monomer transport in the discretized pore space of the evolving agglomerate of microelements is the technique already implemented in our software, we use here the traditional effective-scale approach to monomer transport in the growing polymer particle. The rate of growth of the particular microelement depends on the local concentration of monomer c_i [see Eq. 3 or Eq. A1 (in the Appendix)].

Because the shape of polymer particle can evolve into an arbitrary shape, we define the center of the particle to be identical with the center of the gravity $\boldsymbol{x}_{\text{COG}}$ of the agglomerate of microelements. The characteristic radius of the particle R_{part} is defined as the radius of the sphere with the center at $\boldsymbol{x}_{\text{COG}}$, which contains 95% of all microelements (see Figure 3).

For the sake of simplicity, let us assume: (1) no mass-transport resistance at the surface of polymer particle, (2) uniform distribution of catalyst activity on the effective scale of polymer particle, and (3) establishment of the quasi-stationary profile of concentration inside the polymer particle, that is, the rate of particle growth is considered to be slower than the rate of the reaction–diffusion process. Under these assumptions, the governing reaction–diffusion equation for the monomer concentration c is

$$D^{\text{ef}}\frac{1}{s^2}\frac{d}{ds}\left(s^2\frac{dc}{ds}\right) = k'c_{\text{cat}}c \tag{5}$$

where D^{ef} is the effective diffusivity of monomer in the porous polymer particle, s is the radial coordinate, and c_{cat} is the mass concentration of catalyst per unit volume of polymer particle. The modified rate constant is $k' = k/M_M$, where M_M is the molecular weight of the monomer. The solution of Eq. 5 with the boundary conditions $(dc/ds)|_{s=0} = 0$ and $c|_{s=R_{\text{part}}} = c_{\text{bulk}}$ is

$$\frac{c_i}{c_{\text{bulk}}} = \frac{R_{\text{part}}}{s_i}\frac{\sinh(\Theta s_i/R_{\text{part}})}{\sinh\Theta} \tag{6}$$

where c_i is the monomer concentration at the ith microelement and $s_i = |\boldsymbol{x}_i - \boldsymbol{x}_{\text{COG}}|$ is the distance of the center of the ith microelement $\boldsymbol{x}_i$ from the center of the macroparticle $\boldsymbol{x}_{\text{COG}}$. Parameter $\Theta = R_{\text{part}}\sqrt{k'c_{\text{cat}}/D^{\text{ef}}}$ is the Thiele modulus.

As the polymer particle grows, the catalyst becomes more diluted, that is, $c_{\text{cat}} = c_{\text{cat},0}R^3_{\text{part},0}/R^3_{\text{part}}$, where the subscript 0 stands for the initial value at $t = 0$ s. The Thiele modulus depends on the actual particle radius

$$\Theta = R_{\text{part}}\sqrt{\frac{k'c_{\text{cat}}}{D^{\text{ef}}}} = R^{3/2}_{\text{part},0}\sqrt{\frac{k'c_{\text{cat},0}}{D^{\text{ef}}R_{\text{part}}}} = \Theta_0\sqrt{\frac{R_{\text{part},0}}{R_{\text{part}}}} \tag{7}$$

where Θ_0 is the Thiele modulus at time $t = 0$ s. As the particle and the value of R_{part} grow, the Thiele modulus Θ decreases and therefore the effect of internal diffusion gradually diminishes. Substituting the value of Thiele modulus Θ from Eq. 7 into Eq. 6 allows us to approximate the evolution of monomer profile during the particle growth. Equation 6 could approximate the field of monomer concentration only if the distribution of the catalyst and the porosity on the effective scale of particle are approximately uniform. However, once the macrocavities or cracks are formed in the particle (see below), the applicability of the Eq. 6 approximation is limited.

The detailed discussion of dynamic evolution of the effective-scale concentration profiles, which includes the effect of convective flow driven by the stoichiometry of the polymerization reaction, is given in Kosek et al.[12]

The diffusion limitations arising in the polymerization of HDPE and linear low-density polyethylene (LLDPE) on $TiCl_4/MgCl_2$ catalyst were quantitatively analyzed in experiments by Hamba et al.[37] They found that the effectiveness factor was one for temperatures lower than $T_{\text{div}} = 93°\text{C}$ for HDPE, $T_{\text{div}} = 84°\text{C}$ for LLDPE-10, and $T_{\text{div}} = 72°\text{C}$ for LLDPE-25. Here LLDPE-10 (or LLDPE-25) is the copolymer produced with 10% (or 25%) of propylene in the gas phase. In ethylene copolymerization, the ethylene is more likely to be diffusion limited because its consumption by the reaction is faster and

the center of the growing polymer particle can be ethylene starved. As a result, the comonomer composition across the particle is not uniform, thus leading to heterogeneous comonomer incorporation. This inhomogeneity is most profound at the initial stage of the reaction and, even after 60 min of reaction time, the concentration could still show a 75% difference between the surface and the center of the particle.[37]

Force Interactions among Microelements

The behavior of polyolefins, with respect to their mechanical properties at reaction temperatures, lies between two idealized concepts:

(1) Elastic solid deformation, obeying Hook's law:

$$\sigma = Ee \qquad \text{or} \qquad d\sigma/dt = E(de/dt) \tag{8}$$

(2) Fluid with linear viscous behavior described by the Newton's equation:

$$\sigma = \eta(de/dt) \tag{9}$$

where σ is the stress, e is the strain, E is the elastic modulus, η is the viscosity, and (de/dt) is the strain rate. The Eq. 8 system is applicable only at small strains.

We assume the presence of force interactions of two types acting among individual microelements:

(1) *Binary force interactions*, acting in the normal direction between two connected microelements, which describe the resistance against "push" and "pull" (see Figure 2a).

(2) *Ternary force interactions*, describing the resistance against the change of "bonding angle" in the system of three microelements (see Figure 2c). Alternatively, this type of force interaction could be treated as a binary resistance in the tangential plane[38,39] as implemented in the discrete element modeling of the cohesive powder in the fluidized bed.[40]

Both types of force interactions could be described by several different constitutive equations, such as by Hook's law, by the Maxwell viscoelastic model, or by advanced models using the spectrum of relaxation times (see below). In addition, the proper "stress–strain characteristics" have to be associated with the above- mentioned force interactions to describe the condition for the breakage of the connected microelements.

Binary and ternary force interactions

Let $\boldsymbol{u}$ be the vector connecting microelements A and B, $\boldsymbol{u} = \boldsymbol{x}_B - \boldsymbol{x}_A$, and let F_{AB} be the magnitude of the binary interaction force acting along the connection $\boldsymbol{u}$. Then the force acting on the microelement A is the vector $\boldsymbol{F}_{AB}$

$$\boldsymbol{F}_{AB} = F_{AB}\boldsymbol{u}/|\boldsymbol{u}| \tag{10}$$

The force acting on element B has the opposite direction, $\boldsymbol{F}_{BA} = -\boldsymbol{F}_{AB}$. The positive value of F_{AB} results in the attraction and the negative value in the repulsion of microelements.

Let us describe the relative displacement of microelements A and B in the normal direction by the strain e_{AB}, expressed as

$$e_{AB} = (|\boldsymbol{u}| - u_0)/u_0 \tag{11}$$

where $u_0 = r_A + r_B$ is the equilibrium and $u = |\boldsymbol{u}|$ is the actual distance between the microelements A and B. The constitutive equation describing the force interaction between the microelements A and B has to reflect in the limit of elastic behavior: (1) the nonlinearly increasing repulsion of spheres A and B pushed against each other as the strain e_{AB} is becoming more negative as a result of the increased contact area of spheres A and B, (2) the attraction of spheres A and B connected by the neck of polymer stretched apart for $e_{AB} > 0$, and (3) Hook's law behavior for small absolute values of strain e_{AB}. Therefore the following simple equation, satisfying the requirements listed above, is proposed to calculate the magnitude of the interaction force

$$F_{AB}/A_{AB} = E\,\frac{e_{AB}}{1 + e_{AB}} \tag{12}$$

where the contact area is chosen as $A_{AB} = (1/2)\pi(r_A^2 + r_B^2)$. This choice of contact area A_{AB} is somewhat arbitrary and thus the modulus E is related to the Young's modulus of polymer material only semiquantitatively, but could be calibrated to represent the elastic behavior of the real material. If the microelements are considerably pushed against themselves (that is, $u \ll u_0$), then the strain $e_{AB} \to -1$ and the repulsive force becomes strong. If the microelements are pulled apart then the slope of the stress–strain relationship already becomes weaker for small strains e in the uniaxial tensile tests, as evident for some polyolefin grades, such as in the case of isotactic polypropylene.[41]

Let us now consider the elastic deformation of the triplet of the connected microelements A–V–B. The value of the "bonding" angle ($\alpha = \angle AVB$) at the start of the simulation is assumed to have the equilibrium value α_0. If the translation of the elements leads to the change of the angle then the forces will act on the elements A and B trying to restore the equilibrium angle α_0. The magnitude of the force F_α is proportional to the deviation from the original angle

$$F_\alpha/A_{AB} = -G(\cos\alpha - \cos\alpha_0) \tag{13}$$

where G is the "bending" modulus analogous to Young's modulus used in the binary interaction (Eq. 12). For the sake of simplicity, the choice of the contact area A_{AB} is again the same as above, although the microelements A and B do not have to be in direct contact.

The force F_α acting on the microelements A and B is projected in the direction of the unit vectors $\boldsymbol{w}_a$ and $\boldsymbol{w}_b$ (see Figure 4). Let us define the vectors $\boldsymbol{a} = \boldsymbol{x}_A - \boldsymbol{x}_V$ and $\boldsymbol{b} = \boldsymbol{x}_B - \boldsymbol{x}_V$. The unit vector $\boldsymbol{w}_a$ (or $\boldsymbol{w}_b$) is perpendicular to $\boldsymbol{a}$ (or $\boldsymbol{b}$) and coplanar with the vectors $\boldsymbol{a}$ and $\boldsymbol{b}$, that is

$$\begin{aligned} &\boldsymbol{w}_a \cdot \boldsymbol{a} = 0 \qquad \boldsymbol{w}_a \cdot (\mathbf{a} \times \mathbf{b}) = 0 \qquad |\boldsymbol{w}_a| = 1 \\ &\boldsymbol{w}_b \cdot \boldsymbol{b} = 0 \qquad \boldsymbol{w}_b \cdot (\mathbf{a} \times \mathbf{b}) = 0 \qquad |\boldsymbol{w}_b| = 1 \end{aligned} \tag{14}$$

Unit vectors $\boldsymbol{w}_a$ and $\boldsymbol{w}_b$ are oriented into the convex angle α spanned by vectors $\boldsymbol{a}$ and $\boldsymbol{b}$ (see Figure 4). The forces acting on microelements A and B, that is, $\boldsymbol{F}_{AVB}$ and $\boldsymbol{F}_{BVA}$, have to be compensated by the force $\boldsymbol{F}_{VAB}$ acting on the microelement V

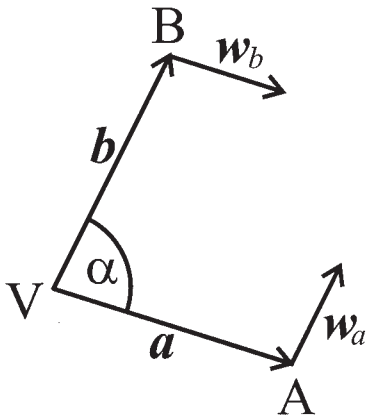

Figure 4. Projection of forces in the triplet of connected microelements *A–V–B* in the direction of unit vectors w_a and w_b.

to prevent the translation movement of the triplet *A–V–B*, expressed as

$$\boldsymbol{F}_{AVB} = F_\alpha \boldsymbol{w}_a \qquad \boldsymbol{F}_{BVA} = F_\alpha \boldsymbol{w}_b \qquad \boldsymbol{F}_{VAB} = -(\boldsymbol{F}_{AVB} + \boldsymbol{F}_{BVA}) \tag{15}$$

The case of co-linear or nearly co-linear vectors $\boldsymbol{a}$ and $\boldsymbol{b}$ is treated in our code in a special way.

Models of viscoelasticity

It is generally accepted that no simple model exists to correctly describe the viscoelastic behavior of semicrystalline polymer solids. Here we shall use the description of viscoelasticity, capturing the essential features of mechanical behavior of polyolefins at typical reactor temperatures. Simple models of viscoelasticity[42] are formed by the formal combination of the elastic spring with modulus E and a viscous dashpot characterized by the viscosity η (see Figure 5).

The *Maxwell model* consists of the spring and the dashpot connected in series. The overall stress σ is the same for both mechanical components. The overall strain e is the sum of the strains of the spring e_1 and of the dashpot e_2, so that $e = e_1 + e_2$. The combination of Eqs. 8 and 9 gives, in the limit of Hook's elasticity,

$$\frac{de}{dt} = \frac{de_1}{dt} + \frac{de_2}{dt} = \frac{1}{E}\frac{d\sigma}{dt} + \frac{\sigma}{\eta} \tag{16}$$

The Maxwell model describes particularly well the relaxation of viscoelastic material subjected to constant strain, that is, $de/dt = 0$. In this case the stress of the material decays exponentially as the piston in the dashpot accommodates to a new position, $\sigma = \sigma_0 \exp(-Et/\eta) = \sigma_0 \exp(-t/\tau_R)$, where σ_0 is the initial stress at $t = 0$ and $\tau_R = \eta/E$ is the relaxation time. The Maxwell model allows for permanent deformation.

The *Voight* (*Kelvin*) *model* consists of the same components as the Maxwell model but connected in parallel (see Figure 5). Equations describing this model are available elsewhere.[42] This model is particularly useful for the description of creep experiments, where the material is subjected to constant loading (stress). The strain then gradually attains the value described by Hook's law and this process is damped by the viscous element.

Although the Maxwell model indicates the general nature of the polymeric behavior under stress, polymeric solids show rather more complex behavior. A more realistic case can be modeled with a continuous or a discrete set of Maxwell elements in parallel.[43] In this case the stress-relaxation modulus $E(t)$, a monotonously decreasing function, can be expressed as

$$E(t) = \sum_{m=1}^{N} E_m \exp(-t/\tau_{R,m}) \tag{17}$$

where $\tau_{R,m}$ represents the relaxation times and E_m is the spectrum of relaxation times. The simple case of Eq. 17 with two parallel Maxwell elements was adopted by Brooks et al.[44] to model mechanical behavior of polyethylene.

Let us illustrate the implementation of these viscoelasticity models into our algorithm. If the Maxwell model is used to describe binary force interactions, then the magnitude of the force between two microelements depends not only on their actual distance, but also on the history of the interaction. For the elastic component (dashpot) described by Eq. 12, the equation analogous to the Maxwell model (Eq. 16) could be derived and the time evolution of the magnitude of force is given by

$$\frac{d(F_{AB}/A_{AB})}{dt} = \frac{[E - (F_{AB}/A_{AB})]^2}{E}\left[\frac{de_{AB}}{dt} - \frac{(F_{AB}/A_{AB})}{\eta}\right] \tag{18}$$

where η is the Maxwell model viscosity parameter that is important for the description of the rate of stress relaxation. The strain rate (de_{AB}/dt) is evaluated as

$$\frac{de_{AB}}{dt} = \frac{u_0 du/dt - u du_0/dt}{u_0^2}$$

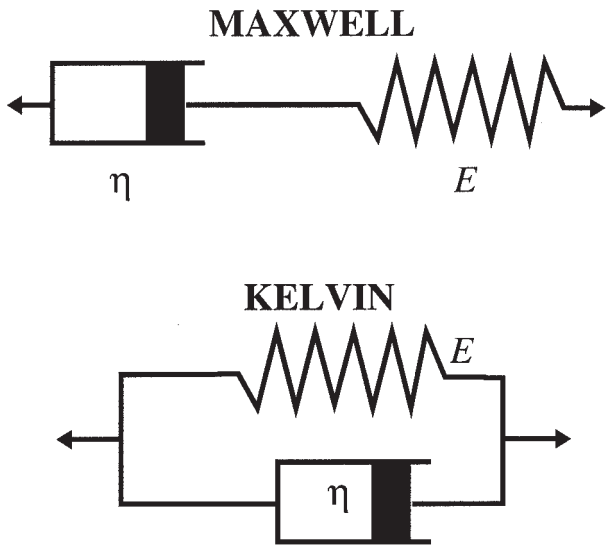

Figure 5. Maxwell and Kelvin models of viscoelasticity.

where $u = |\mathbf{u}|$

$$\frac{du}{dt} = \frac{(\boldsymbol{x}_B - \boldsymbol{x}_A)\cdot(\boldsymbol{v}_B - \boldsymbol{v}_A)}{u} \tag{19}$$

and $(du_0/dt) = dr_A/dt + dr_B/dt$.

In practice, viscoelastic properties of polymeric materials are often characterized by tools of dynamic mechanical testing. The polymer specimen is subjected to a variable loading at a moderately high frequency, such as when an oscillating sinusoidal load is applied to a polymer at a particular angular frequency ω. For the viscoelastic material, the strain lags somewhat behind the applied stress and this can be considered as the manifestation of the damping process. Let the relative angular displacement (that is, the phase lag) of stress and strain be denoted as δ. Then the variation of stress and strain with time is given by the following expressions

$$\sigma = \sigma_0 \sin(\omega t + \delta) \qquad e = e_0 \sin \omega t \tag{20}$$

The stress σ could be resolved into one component, which is in phase with the strain and is characterized by the storage modulus $E' = (\sigma_0/e_0)\cos\delta$, and another component, which is $\pi/2$ out of phase with the strain and is characterized by the loss modulus $E'' = (\sigma_0/e_0)\sin\delta$,

$$\sigma = e_0 E' \sin \omega t + e_0 E'' \cos \omega t \tag{21}$$

and for the phase lag we have $\tan\delta = E''/E'$.

Stress–strain characteristics and connectivity of microelements

The computational algorithm keeps the list of the connected pairs of neighboring microelements and the list of the connected triplets of microelements. This list is updated, that is, new connections are created or existing connections are broken in each step of the dynamic simulation. The suitable set of rules for the creation/deletion of the microelement bonds has to be defined.

The microelements A and B become connected when they touch each other, that is, their distance $u = |\boldsymbol{u}|$ becomes

$$|\boldsymbol{u}| \le u_0 = r_A + r_B \tag{22}$$

Two elements become disconnected if their distance exceeds maximum strain $e_{\max}$

$$e_{AB} = \frac{|\boldsymbol{u}| - u_0}{u_0} > e_{\max} \tag{23}$$

The microelements in the distance $u \in [u_0, (1 + e_{\max})u_0]$ could thus be either connected or disconnected depending on their previous trajectory. Thus a simple dilatational hysteresis is considered. The rule of thumb estimates the maximum tensile strength to be $\sigma_t \approx E/10$, where E is the elastic modulus.[42] The tensile yield strain increases as the crystallinity of polyethylene sample is reduced.[45]

The triplet A–V–B is initiated when both the connection A–V and the connection B–V are formed and it disappears if:

(1) one of the connections A–V or B–V is disconnected, or

(2) the deviation between the actual angle $\alpha = \angle AVB$ and the initial angle α_0 exceeds the limiting value $\alpha_{\max}$

$$|\alpha - \alpha_0| > \alpha_{\max} \tag{24}$$

In this latter case one of the connections A–V and B–V is also disconnected.

The stress–strain characteristics of polymers measured by ASTM or ISO tests are not suitable for the estimation of maximum elongation strain $e_{\max}$ and the maximum bending angle difference $\alpha_{\max}$ because they are measured at room temperature in the limit of a very slow deformation. Therefore the parameters $e_{\max}$ and $\alpha_{\max}$ are chosen empirically in this study.

Moreover, the measured stress–strain curves do not describe the reversible processes. When the applied strain is large, then only the elastic component of the deformation is reversed, but the plastic deformation remains. A perfect model would: (1) conform with Hook's law for small strains, (2) describe the brittle behavior or necking of polymer at larger strains, (3) describe properly the plasticity of the material, and (4) describe the breakup of the material at large strains. Inevitably, such a model would be complicated. Our model uses the requirements listed above reasonably well in terms of the considered stress. Various types of tensile behavior (such as necking or brittleness) could be roughly approximated by adjusting the maximum elongation parameter $e_{\max}$ in Eq. 23. The values of maximum deformations $e_{\max}$ and $\alpha_{\max}$ used herein are relatively small and thus the stress–strain characteristics of polyolefins can be oversimplified.

Qualitative Analysis of the Morphogenesis Model

The purpose of the following section is not the transformation of model equations into dimensionless form as it may seem. Such a transformation is just optional before writing the computer program. However, the principal equations in the dimensionless form allow us to qualitatively understand the behavior of the morphogenesis model and the corresponding principal parameters.

Let us introduce the dimensionless parameters of the ith microelement: position $\boldsymbol{X}_i$, velocity $\boldsymbol{V}_i$, radius R_i, concentration of surrounding monomer C_i, and the mass of catalyst $M_{\mathrm{cat},i}$, as well as the dimensionless time τ, defined as

$$\boldsymbol{X}_i = \boldsymbol{x}_i/R_0 \qquad \boldsymbol{V}_i = \boldsymbol{v}_i\tau_0/R_0 \qquad R_i = r_i/R_0$$

$$C_i = c_i/c_{\mathrm{bulk}} \qquad M_{\mathrm{cat},i} = m_{\mathrm{cat},i}/m_{\mathrm{cat},0} \qquad \tau = t/\tau_0 \tag{25}$$

where R_0, τ_0, c_{bulk}, and $m_{\mathrm{cat},0}$ are, respectively, the characteristic length, time, monomer concentration, and mass of catalyst, where the characteristic length R_0 is the typical or initial radius of the microelement.

Analysis of the growth of microelements

Only the simplified case of nonoverlapping spherical elements is discussed in this section. Substitution of dimension-

less variables into Eqs. 3 and 2 gives the growth rate of the dimensionless microelement radius $dR_i/d\tau$

$$\frac{dR_i}{d\tau} = \frac{km_{\text{cat},0}c_{\text{bulk}}\tau_0}{\rho_i 4\pi R_0^3}\frac{M_{\text{cat},i}C_i}{R_i^2} = \Gamma\frac{M_{\text{cat},i}C_i}{R_i^2} \tag{26}$$

where the value of the dimensionless parameter Γ, which characterizes the growth, could be computed from the polymer yield rate A_Y in $kg_{pol}/(g_{cat}\ h)$ (see the discussion after Eq. 3). Thus, according to Eq. 26, the growth of the microelement depends on its size, on the concentration of the surrounding monomer, and on the amount of active catalyst sites inside the ith microelement. The analytical solution of Eq. 26 in the case of the constant value of the surrounding monomer concentration C_i and constant catalyst activity is

$$R_i^3 = R_{0,i}^3 + 3\Gamma M_{\text{cat},i}C_i\tau \tag{27}$$

where $R_{0,i}$ is the initial dimensionless radius of the ith microelement. It could be further shown that in the case of catalyst mass proportional to the initial microelement volume, that is, $M_{\text{cat},i} = (4/3)\pi R_0^3 R_{0,i}^3 \rho_i w_{\text{cat}}/m_{\text{cat},0}$, Eq. 27 simplifies further into

$$R_i^3 = R_{0,i}^3(1 + 3\Gamma' C_i\tau) \tag{28}$$

where $\Gamma' = \Gamma(4/3)R_0^3\pi\rho_i w_{\text{cat}}/m_{\text{cat},0}$ is the modified dimensionless growth parameter and w_{cat} is the initial weight fraction of the catalyst in each microelement.

Equation 28 has important consequences. In the limit of packed agglomerate of microelements surrounded by the same monomer concentration and with the same initial fraction of active catalyst sites in microelements, the growth of microelement volumes is going to be linear in time. Let us imagine the trivial case of the network of connected (touching) spherical microelements with a distribution of initial radii $R_{0,i}$. As the microelements grow, all connections among the microelements are elongated at the same rate and also all "bonding" angles of triplets of microelements remain without change. Therefore no deformations affecting the morphology of the agglomerate of microelements are going to occur according to these geometrical arguments.

The above-mentioned consequences are in contrast to the approach of Kittilsen et al.,[46] who considered pseudo-homogeneous effective mechanical properties in the polymer particle, and where the local volume change of polymer particle results in a localized stress in the material. As shown below, only uneven growth rates of microelements result in the buildup of stress in the particle.

Analysis of the elastic deformation

The substitution of dimensionless variables from Eq. 25 into the Eq. 1 system, describing the translation motion of the ith microelement, gives

$$\frac{d\boldsymbol{X}_i}{d\tau} = \boldsymbol{V}_i \tag{29}$$

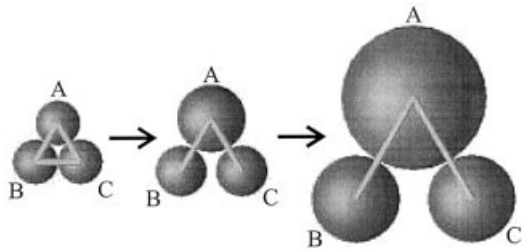

Figure 6. Effect of the nonuniform distribution of catalyst activity in microelements on the growth of three connected microelements.

The connection between the microelements B and C is ruptured in the process of growth because of the imposed resistance against the change of bonding angle.

$$\rho_i 4\pi R_i^2\frac{dR_i}{d\tau}\boldsymbol{V}_i + \rho_i\frac{4}{3}\pi R_i^3\frac{d\boldsymbol{V}_i}{d\tau} = \frac{\tau_0^2}{R_0^4}\left(\sum_j \boldsymbol{F}_{ij}^{\text{binary}} + \sum_{j,k}\boldsymbol{F}_{ijk}^{\text{ternary}}\right) \tag{30}$$

and Eq. 30 could be rearranged after the substitution of the microelement growth rate $dR_i/d\tau$ given by Eq. 26 and the microelement radius given by Eq. 27 into

$$\Gamma M_{\text{cat},i}C_i\boldsymbol{V}_i + \frac{1}{3}(R_{0,i}^3 + 3\Gamma M_{\text{cat},i}C_i\tau)\frac{d\boldsymbol{V}_i}{d\tau} = \frac{\tau_0^2}{\rho_i 4\pi R_0^4}\boldsymbol{F}_i^{\text{sum}} \tag{31}$$

where $\boldsymbol{F}_i^{\text{sum}}$ is the summation of all force interactions acting on the ith microelement. Equation 31 stresses the importance of the nonuniform distribution of catalyst activity $M_{\text{cat},i}$ and initial radii $R_{0,i}$ among the microelements, which is the important effect that has not been addressed yet in the previous works done in the framework of the multigrain model. The importance of the effect of concentration field C_i on the trajectory of the ith microelement is also evident.

Let us illustrate the effect of the nonuniform distribution of catalyst activity in microelements in the simple case of three connected microelements (see Figure 6). The initial sizes of microelements A, B, and C are the same, $R_{0,A} = R_{0,B} = R_{0,C}$, but the loading of catalyst is different, $M_{\text{cat},A} = 2M_{\text{cat},B} = 2M_{\text{cat},C}$.

The only information required to calculate the magnitude of the binary elastic force between the elements is their position and radii. The magnitude of the elastic force is given by the constitutive Eq. 12 and its transformation into dimensionless variables (Eq. 25) is

$$\boldsymbol{F}_{ij}^{\text{binary}} = EA_{ij}\frac{e_{ij}}{1+e_{ij}}\boldsymbol{w}_{ij} = E\pi R_0^2\frac{R_i^2 + R_j^2}{2}\boldsymbol{\varepsilon}_{ij} \tag{32}$$

where $\boldsymbol{w}_{ij}$ is the projection vector and $\boldsymbol{\varepsilon}_{ij}$ is the projected strain. Similarly, the ternary interaction Eq. 13 is transformed with the use of Eq. 25, as follows

$$\boldsymbol{F}_{ijk}^{\text{ternary}} = -GA_{ij}(\cos\alpha - \cos\alpha_0)\boldsymbol{w}_{ijk} = G\pi R_0^2\frac{R_i^2 + R_j^2}{2}\boldsymbol{\varepsilon}_{ijk} \tag{33}$$

where $\boldsymbol{w}_{ijk}$ is the projection vector and $\boldsymbol{\varepsilon}_{ijk}$ is the projected strain.

Thus the terms corresponding to binary and ternary elastic interactions on the righthand side of Eq. 31 are

$$\frac{\tau_0^2}{\rho_i 4\pi R_0^4}\sum_j \boldsymbol{F}_{ij}^{\text{bin.}} = \frac{E\tau_0^2}{\rho_i 4R_0^2}\sum_j \frac{R_i^2+R_j^2}{2}\boldsymbol{\varepsilon}_{ij} = \Psi_E \sum_j \frac{R_i^2+R_j^2}{2}\boldsymbol{\varepsilon}_{ij} \tag{34}$$

$$\frac{\tau_0^2}{\rho_i 4\pi R_0^4}\sum_{j,k} \boldsymbol{F}_{ijk}^{\text{tern.}} = \frac{G\tau_0^2}{\rho_i 4R_0^2}\sum_{j,k} \frac{R_i^2+R_j^2}{2}\boldsymbol{\varepsilon}_{ijk} = \Psi_G \sum_{j,k} \frac{R_i^2+R_j^2}{2}\boldsymbol{\varepsilon}_{ijk} \tag{35}$$

where Ψ_E and Ψ_G are, respectively, the dimensionless elastic and bending moduli. The term $R_i^2 + R_j^2$ could be substituted from Eq. 27 to give

$$R_i^2 + R_j^2 = R_{0,i}^3 + 3\Gamma M_{\text{cat},i}C_i\tau)^{2/3} + (R_{0,j}^3 + 3\Gamma M_{\text{cat},j}C_j\tau)^{2/3} = R_{\Gamma,i}^2 + R_{\Gamma,j}^2 \tag{36}$$

A combination of Eqs. 31, 34, 35, and 36 gives

$$\boldsymbol{V}_i + \left(\tau + \frac{R_{0,i}^3}{\Gamma M_{\text{cat},i}C_i}\right)\frac{d\boldsymbol{V}_i}{d\tau} = \frac{\Psi_E}{\Gamma M_{\text{cat},i}C_i}\sum_j \frac{R_{\Gamma,i}^2+R_{\Gamma,j}^2}{2}\boldsymbol{\varepsilon}_{ij} + \frac{\Psi_G}{\Gamma M_{\text{cat},i}C_i}\sum_{j,k}\frac{R_{\Gamma,i}^2+R_{\Gamma,j}^2}{2}\boldsymbol{\varepsilon}_{ijk} \tag{37}$$

Further analysis of the deformations is possible in the simple situation of a few interacting microelements. Such an analysis involves simultaneous solution of Eq. 37 for several connected microelements. The solution of the deformation Eq. 37 is going to depend on the ratio of the dimensionless elastic (and bending) modulus to the dimensionless growth rate of microelements, that is, on the ratios $\Psi_E/(\Gamma M_{\text{cat},i}C_i)$ and $\Psi_G/(\Gamma M_{\text{cat},i}C_i)$.

To summarize, the parametric space of the introduced morphogenesis model, with respect to the simple elastic interactions, is ample because it includes: growth parameter Γ, dimensionless elastic and bending moduli Ψ_E and Ψ_G, maximum elongation strain $e_{\max}$ and maximum change of bonding angle $\alpha_{\max}$, distributions of initial radii $R_{0,i}$ and catalyst loading $M_{\text{cat},i}$ of microelements, and the evolving concentration field C_i. The initial exploration of such a vast parametric space has to be driven more by intuition and by the knowledge of relevant experimental facts than by systematic approach.

Analysis of the viscoelastic interaction

To derive the dimensionless equation for the viscoelastic Maxwell force we start from Eq. 16, substitute $\sigma = F_{ij}/A_{ij}$ for the stress, and express the time derivative of the binary force dF_{ij}/dt to the lefthand side as

$$\frac{dF_{ij}}{dt} = EA_{ij}\frac{de_{ij}}{dt} + F_{ij}\left(\frac{1}{A_{ij}}\frac{dA_{ij}}{dt} - \frac{E}{\eta}\right) \tag{38}$$

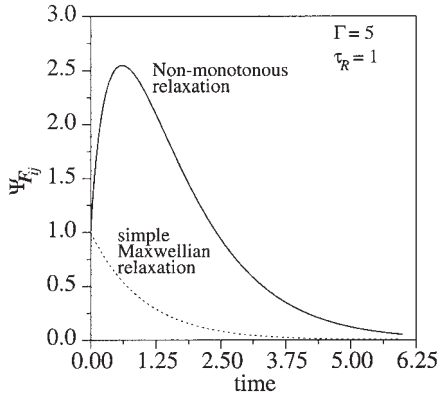

Figure 7. Nonmonotonous relaxation of the Maxwell model in the case of the growing microelements described by Eq. 41.

This equation could be transformed into the dimensionless form with the use of transformations (Eq. 25), whereupon we obtain

$$\frac{d\Psi_{F_{ij}}}{d\tau} = \frac{\pi}{2}(R_i^2+R_j^2)\frac{de_{ij}}{d\tau} + \Psi_{F_{ij}}\left[\frac{2}{R_i^2+R_j^2}\left(R_i\frac{dR_i}{d\tau}+R_j\frac{dR_j}{d\tau}\right) - \frac{1}{T_R}\right] \tag{39}$$

where $\Psi_{F_{ij}}$ is the dimensionless force and $\mathcal{T}_R = \eta/(E\tau_0)$ is the dimensionless relaxation time. Let us substitute for the rate of growth $dR_i/d\tau$ and $dR_j/d\tau$ of microelements i and j from Eq. 26, and let us substitute for R_i and R_j from Eq. 27. Let us further simplify the discussion to the case of two equivalent microelements, that is, $R_i = R_j$, $M_{\text{cat},i} = M_{\text{cat},j}$, and $C_i = C_j$. Then Eq. 39 is transformed into

$$\frac{d\Psi_{F_{ij}}}{d\tau} = \pi R_i^2\frac{de_{ij}}{d\tau} + \Psi_{F_{ij}}\left(\frac{2\Gamma M_{\text{cat},i}C_i}{R_{0,i}^3(1+3\Gamma M_{\text{cat},i}C_i\tau)} - \frac{1}{\mathcal{T}_R}\right) \tag{40}$$

The first term on the right-hand side describes the rate of the built-up force ("stress accumulation") resulting from the relative movements of microelements and the growth of microelements. The first term in parentheses corresponds to the buildup of tension arising from the growth of the contact area between microelements and the last term with $\mathcal{T}_R$ describes the force relaxation.

Let us investigate the evolution of the interaction force F_{ij} in the relaxation experiment with the constant strain $de_{ij}/dt = 0$ and with the characteristic spatial scale R_0 set to the initial radius of the microelement, so that $R_{0,i} = 1$. In this case the analytic solution of Eq. 40 becomes

$$\Psi_{F_{ij}} = \Psi_{F_{ij,0}}(1+3\Gamma M_{\text{cat},i}C_i\tau)^{2/3}\exp(-\tau/\mathcal{T}_R) \tag{41}$$

Let us note that the force $\Psi_{F_{ij}}$ in Eq. 41 is evolving nonmonotonously, unlike the simple Maxwellian relaxation $\Psi_{F_{ij}} = \Psi_{F_{ij,0}}\exp(-\tau/\mathcal{T}_R)$ (see Figure 7). The reason for the nonmonotonous evolution of force is the rate of growth of microelements resulting in the increased interaction area A_{ij} of two

overlapping microelements kept in the distance corresponding to constant strain e_{ij}. The rate of Maxwellian relaxation of repulsive forces among microelements is going to affect the evolution of the porosity of polymer particle.

Results of Modeling of Morphogenesis of Polyolefin Particles

The effective-scale models of the particle growth, including the multigrain model, can be criticized for the avoidance of the fragmentation stage of the particle evolution. The initial condition in these models is usually a hypothetical perfect multigrain morphology in the early stage of particle growth just after the complete fragmentation of the catalyst support.

We are not bound to such simplifications with our class of models when at least two types of microelements corresponding to the polymer and catalyst phase are considered. However, to keep the model used herein simple and the parametric space focused, we use only one type of microelement equivalent to a single micrograin or to a cluster of micrograins in the multigrain morphology. The sintering of microelements during their growth could provide morphologies different from that of the perfect multigrain. The starting point of our simulation is therefore also the idealized state of the catalyst/polymer particle just after the fragmentation. A more complex approach is used in the ongoing work on the dynamics of particle fragmentation.

We explore the possibilities resulting from the combination of particle growth, mass-transport resistances, nonuniform distributions of catalyst activities, and viscoelastic properties of polyolefins. Our aim is to predict the experimentally observed morphologies of polyolefin particles, which is hardly possible by effective-scale models of particle growth. However, we are well aware that the formation of various morphologic features could be explained in alternative ways.

The model is formulated and coded in three spatial dimensions (3-D), but we present the results obtained with the model mostly in spatially two-dimensional (2-D) situations because 2-D results are more illustrative. The extrapolation of simulated morphogenetic behaviors from 2-D into 3-D has to be carried out with caution because of the larger number of connections with neighboring elements in the 3-D case. Dynamic simulations with the number of microelements on the order of 10^4 are reasonably fast. However, the default initial conditions sufficient for illustrative purposes are represented by a circle with nearly 600 regularly ordered microelements of the same diameter in the 2-D case and a sphere with a few thousand of microelements in the 3-D case.

Purely elastic interactions of microelements combined with mass-transport resistance

Let us start with a simple case of purely elastic interactions among microelements described by the modified Hook's law (Eq. 12) and its analog describing the resistance against bending in the system of three microelements (Eq. 13). The agglomerate of microelements could be visualized in this case by a number of nodes connected by undamped springs. Such a model contains no means for the dissipation of mechanical energy introduced into the system by the displacement of microelements from their initial positions because of the growth and mutual interactions among them. Each microelement therefore oscillates around its equilibrium position and thus the purely elastic interactions do not describe realistic behavior. Viscous dashpots available in Maxwell, Kelvin (Voight), or more advanced models of viscoelasticity are capable of absorbing the mechanical energy and thus cause the damping of oscillating microelements.

Table 1. Default Values of Model Parameters

Parameter	Default Value
Catalyst activity A_Y	36 $kg_{pol}/(g_{cat}\ h)$
Effective diffusivity D^{ef}	10^{-8} m^2/s
Density ρ	960 kg/m^3
Young modulus E	100 MPa
Bending moduls G	$G = 0.2E$
Characteristic time τ_0	1 s
Characteristic length R_0	1 μm
Characteristic concentration of monomer c_{bulk}*	681 mol/m^3
Characteristic mass of catalyst	$m_{cat,0}$
Initial microelement radius $R_{0,i}$	$R_{0,i} = 1$
Initial particle radius $R_{part,0}$	24 μm
Growth factor Γ	3.3
Initial Thiele number Θ_0	5.6
Modulus Ψ_E**	$2.5 \times 10^8 E$
Modulus Ψ_G**	$2.5 \times 10^8 G$
Maximum strain e_{max}	0.04, 0.09, or 0.24
Maximum bending α_{max}	5° or 15°
Mass of catalyst in microelement $M_{cat,i}$	1

*Calculated from the ideal equation of state at temperature 80°C and pressure 20 bar.
**The values of Ψ_E and Ψ_G used in simulations are smaller (see text).

The frequency of oscillations of individual microelements subjected to purely elastic interactions is large because of their small mass. Therefore the Kelvin-like damping has to be implemented in the integration method. The significant interpenetration of microelements is unlikely in the case of purely elastic interactions.

When all microelements grow at the same rate (and the weight fraction of catalyst in microelements is the same) then the initial configuration (that is, relative mutual positions of microelements) is going to be preserved. In this case, the growth process replicates the initial shape and morphology. The nonuniform growth of microelements could be caused (such as by the mass-transport resistance in the growing particle) as discussed above in the introduced model. The microelements located in the center of the particle grow more slowly than those at the surface of the particle as a result of the nonuniformity of the monomer concentration field. Therefore the tension in the particle grows gradually and, after some time, cracks can occur inside the particle. The movement of the ith microelement is described by Eq. 37, which considers the dependency of movement on the dimensionless growth factor Γ and the dimensionless concentration of monomer C_i.

Default values of model parameters are summarized in Table 1. The initial distribution of catalyst in the microelements of the same size is considered to be uniform and the selection of the maximum strain e_{max} and the maximum bending α_{max} is based on the arguments given in the short discussion of stress–strain characteristics.

The dimensionless growth factor Γ could be simply calculated as $\Gamma = \tau_0 (A_Y \rho_{part,0}/\rho_{part,3600})/(3 \times 3.6)$, where the unit of catalyst activity is $[A_Y] = kg_{pol}/(g_{cat}\ h)$, $\rho_{part,0}$ is the initial density of particle, and $\rho_{part,3600}$ is the density at $t = 3600$ s.

Thus the dimensionless growth factor $\Gamma \doteq 3.3$ for $A_Y = 36$ $kg_{pol}/(g_{cat}\ h)$ and $\rho_{part,0}/\rho_{part,3600} = 1$.

The monomer concentration profile is parameterized by the Thiele modulus Θ, which decreases as the particle grows (see Eqs. 6 and 7). In the limit of $\Theta \to 0$ the ratio $(c|_{s=0}/c_{bulk}) = 1$ and all microelements grow uniformly. In the opposite limit $\Theta \to \infty$ the ratio $(c|_{s=0}/c_{bulk}) = 0$ and the microelements in the center of the particle do not grow at all. In the case of polymerization with effective diffusivity $D^{ef} = 10^{-8}$ $m^2\ s^{-1}$ and catalyst activity $A_Y = 36$ $kg_{pol}/(g_{cat}\ h)$ the initial Thiele modulus $\Theta_0 = \Theta(t = 0) \doteq 5$ and thus the initial ratio $(c|_{s=0}/c_{bulk}) \doteq 0.07$.

The selected values of characteristic parameters (see Table 1) lead to the dimensionless Young's modulus $\Psi_E = 2.5 \times 10^8 E$ and $\Psi_G = 2.5 \times 10^8 G$, respectively. The typical values of Young's modulus E and bending modulus G are on the order of 100 MPa, and thus the dimensionless moduli Ψ_E and Ψ_G are large numbers of the order 10^{16}. This makes the purely elastic problem practically unsolvable by usual numerical methods because of the tiny time step required to capture the dynamics of elastic interactions. Large values of Ψ_E predetermine the large frequency of induced oscillations of microelements. Therefore the values of Ψ_E and Ψ_G are significantly reduced ($\Psi_E \approx 10^5$, $\Psi_G \approx 10^5$) to make the dynamic simulation computationally feasible. In the purely elastic regime the results of morphogenetic simulations do not depend on the actual value of Ψ_E provided this value is sufficiently large, that is $\Psi_E \gg \Gamma$. The main purpose of elasticity in the purely elastic regime is to keep the configuration (that is, the connections among microelements) and to provide the stress field in the growing particle. The stress is built up instantaneously as the particle grows and depends only on the positions of microelements in the case of purely elastic interactions. The rate of growth of individual microelements is affected by the mass-transport resistance described by the Thiele modulus Θ.

The formation of various morphological patterns in the course of the particle growth is illustrated in Figures 8–12. The resulting morphologies could be classified qualitatively into several types:

(1) *Compact particle*. The compact morphology describes the situation of the perfect replication of the initial particle structure, such as at conditions of small mass-transport limitations (small Θ; see Figure 8).

(2) *Macrocavities*. The particle remains compact, but the large macrocavities are formed. In the situation shown in Figure 9 the particle lost its spherical (circular) shape as it grew.

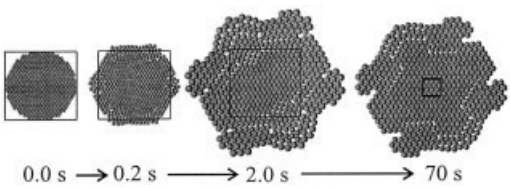

Figure 8. Morphogenesis and growth of the compact polymer particle.

Polymer yield $A_Y = 36$ $kg_{pol}/(g_{cat}\ h)$, no ternary interactions, $e_{max} = 0.09$, $\Theta_0 = 5.6$. The rectangle shows the relative spatial scale of the growing particle.

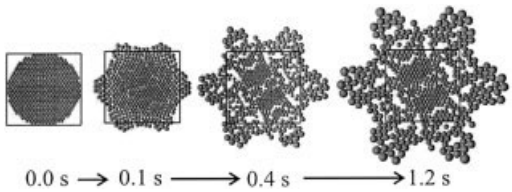

Figure 9. Morphogenesis and growth of particle with macrocavities.

Polymer yield $A_Y = 100$ $kg_{pol}/(g_{cat}\ h)$, no ternary interactions, $e_{max} = 0.02$, $\Theta_0 = 9.3$. The rectangle shows the relative spatial scale of the growing particle.

(3) *Hollow particle*. In this case one large macrocavity is formed in the center of the particle (see Figure 10). The empty area in the center of the particle relatively reduces its size as the particle grows for long simulation times as the Thiele modulus Θ decreases.

(4) *Disintegration into fines*. The particle has disintegrated into several fragments during its growth (see Figure 11).

(5) *Attrition of microelements*. Small fragments disintegrate and are ripped off from the particle surface (see Figure 12). This situation arises in the case of the weak triplet interactions (low ratio G/E) and the "unflexible" bonds characterized by the small value of α_{max}.

Let us note that the fines do not form unless the ternary interactions characterized by the bending modulus G and parameter α_{max} are present. However, the macrocavities could also form inside the growing particle in the case $G = 0$ and $\alpha_{max} = 180°$, that is, in the case without ternary interactions.

The smaller the maximum strain e_{max} and α_{max} (that is, the more brittle the particle), the earlier the formation of cracks. As the initial Thiele modulus Θ_0 diminishes, the concentration profile inside the particle becomes more uniform and the first rupture of the connection between the microelements is going to be delayed. In the limiting case of the uniform growth of microelements (with uniform catalyst concentration) the particle is never going to crack.

In the case of a strong ternary interaction, a hollow particle is likely to be formed. On the other hand when the ratio G/E is small, then the particle can disintegrate into several fines during its growth. Let us also note that the shape of the particle need not be perfectly replicated during its growth, especially in the case of significant mass-transport limitation inside the particle (see Figure 13).

The 3D morphologies show features similar to those of 2D morphologies (see Figure 14), with the illustrative examples of

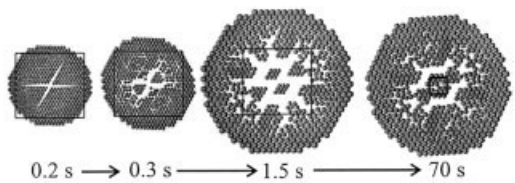

Figure 10. Formation of the hollow particle caused by mass-transport limitations.

Polymer yield $A_Y = 36$ $kg_{pol}/(g_{cat}\ h)$, ternary interactions with bending modulus $G = 10E$, $\alpha_{max} = 5°$, $e_{max} = 0.09$, $\Theta_0 = 5.6$. The rectangle shows the relative spatial scale of the growing particle.

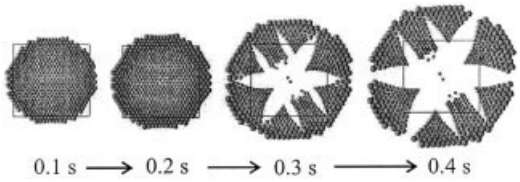

Figure 11. Disintegration of the particle into fines during its growth.

Polymer yield $A_Y = 100\ kg_{pol}/(g_{cat}\ h)$, ternary interactions with bending modulus $G = E$, $\alpha_{max} = 15°$, $e_{max} = 0.24$, $\Theta_0 = 9.3$. The rectangle shows the relative spatial scale of the growing particle.

spatially 3-D morphologies developed in the case of purely elastic interactions among microelements. The tendency of growing particles to disintegrate is reduced in 3-D simulations because the coordination number of microelements (that is, the number of connection with neighbors) is larger than that in the 2-D case. Hollow particles are formed in 3-D even for $G = E$, whereas in 2-D the formation of hollow particles has been observed only with $G \geq 10E$.

Maxwell interactions of microelements combined with mass-transport resistance

The previous section has shown that even the simple case of elastic force interactions acting among individual microelements provides a rich behavior, including the formation of macrocavities in particles, hollow particles, fines, and imperfect replications of particle shape during its growth. Let us now approximate the viscoelastic behavior of polyolefins by a simple Maxwell model. Thus the relaxation of the built-up stress, that is, the "accommodation" of the system to the permanent deformation, can be simulated.

The parameter characterizing the relaxation is τ_R, which is varied from $\tau_R \to \infty$ (elastic limit) to $\tau_R = 0.01$ s (fast relaxation). The typical value of τ_R at reaction temperatures is between 0.1 and 3 s.

Results of simulations performed with different values of Maxwellian relaxation times τ_R are illustrated in Figure 15. The behavior of the system in the limit $\tau_R \to \infty$ is elastic. As the rate of the stress relaxation increases, the occurrence of the first rupture (of the connection between the microelements) is delayed and fast relaxation reduces the formation of ruptures. With the increasing rate of relaxation the morphology of the particle changes from the formation of fines, through the formation of macrocavities and hollow particles, up to the formation of the nearly compact particle. The relaxation also affects the particle porosity and shape.

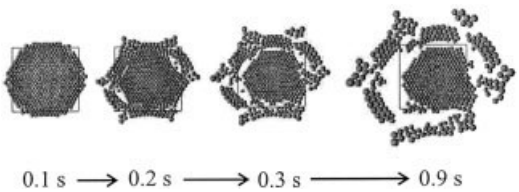

Figure 12. Attrition from the particle surface during the particle growth.

Polymer yield $A_Y = 100\ kg_{pol}/(g_{cat}\ h)$, ternary interactions with bending modulus $G = 0.2E$, $\alpha_{max} = 5°$, $e_{max} = 0.24$, $\Theta_0 = 9.3$. The rectangle shows the relative spatial scale of the growing particle.

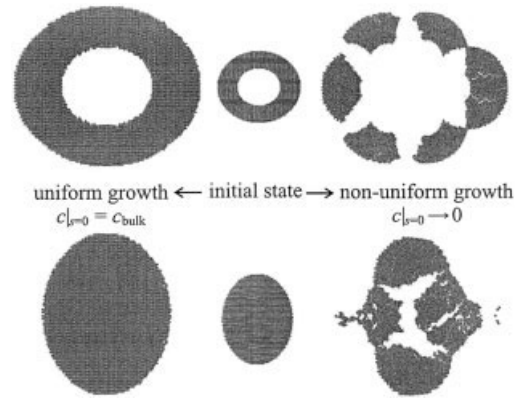

Figure 13. Examples of the poor replication of the particle shape during its growth.

No ternary interactions, $e_{max} = 0.04$. The Thiele number is kept constant during the particle growth.

Figure 15 illustrates the complex interplay between the particle growth (characterized by $\Gamma \sim A_Y$), relaxation of stress (characterized by τ_R), and mass-transport limitation (characterized by the initial value of Thiele modulus Θ_0). The rate of the stress buildup is proportional to the uneven rate of growth of microelements, even when the simple relaxation is considered (see Figure 7 and Eq. 41). Most significant morphological

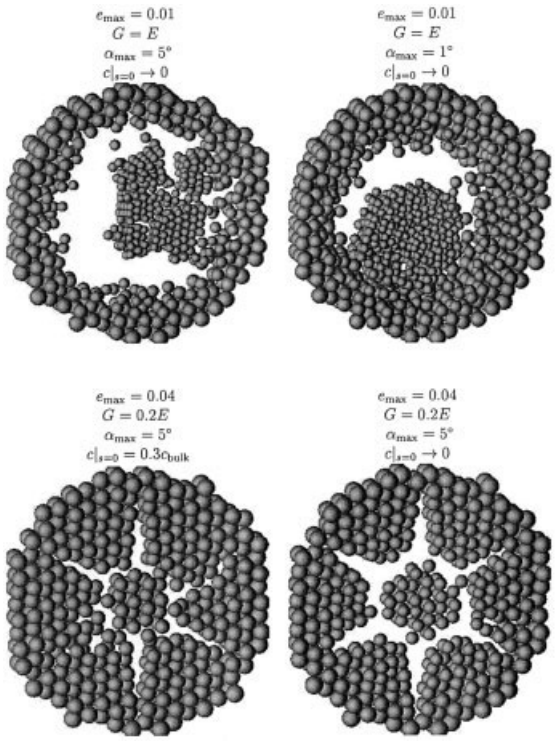

Figure 14. Illustrative examples of spatially 3D morphologies.

Resulting structures are hollow particles and macrocavities. For better visualization, only the thin section taken from the middle part of the particle is displayed. The Thiele number is kept constant during the particle growth.

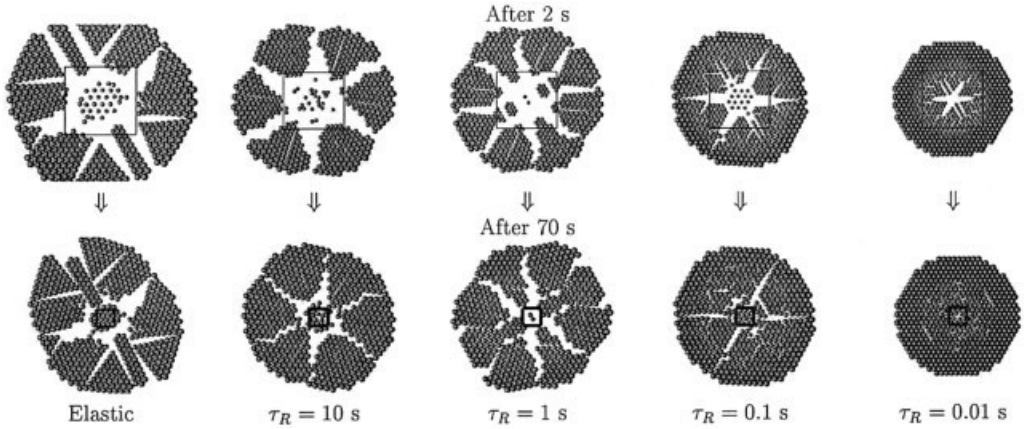

Figure 15. Effect of the relaxation time τ_R (in the Maxwell model) on the resulting morphology.

Polymer yield $A_Y = 36$ $kg_{pol}/(g_{cat}$ h), ternary interactions with the bending modulus $G = 0.2E$, $\alpha_{max} = 5°$, $e_{max} = 0.04$, $\Theta_0 = 5.6$. The rectangle shows the relative spatial scale of the growing particle.

changes occur in the early stage of particle growth, where the rate of relative displacement of microelements caused by the growth is large (see Eqs. 27 and 37). This can be seen also in Figure 15.

Contrary to the elastic model, where the microelements are well separated, the Maxwell model allows for permanent deformation including partial interpenetration of neighboring microelements. For example, the microelements in the outer shells of the particle are pushed together in the detailed Figure 16.

The effect of the mass-transport resistance on the morphogenesis of the polymer particle is illustrated in Figure 17. The small value of the initial Thiele modulus $\Theta_0 = 2.5$ gives the compact morphology, the larger value $\Theta_0 = 4.0$ yields macrocavities and cracks, and the large value $\Theta_0 = 5.6$ causes the particle to disintegrate into fines at time $t = 0.5$ s.

Effect of the nonuniform distribution of catalyst activity

The resulting morphologies described so far originated from the initial conditions represented in the 2-D case by a circle with regularly ordered microelements of the same diameter containing the same amount of catalyst. However, the real structure of the initial agglomerate of microelements is irregular. The irregularity could be simply introduced into initial conditions, such as by the random removal of microelements or by the consideration of the nonuniform distribution of catalyst activity in microelements. The introduction of these irregularities reduces the time of the first rupture (that is, of the disconnection of microelements) in the growing particle and enhances the tendency to the formation of disordered morphologies, such as macrocavities and fines.

Let us first randomly remove about 5% of the microelements from the initial conditions (see Figure 18). In the case of a relatively tough particle (with higher value of e_{max}) the replication of the particle shape is observed and no fractures are formed (see Figure 18a, which displays the situation at time $t =$ 2 s). As the value of the maximum strain e_{max} is reduced (toward a more brittle polymer), the irregularities cause the formation of macrocavities (see Figure 18b). Let us note that no macrocavities are formed for initially compact particle at the same conditions. Irregularities in initial conditions also affect the shape and the number of fragments (Figure 18c) and they reduce the symmetry of fractures (Figure 18d).

The size of fragments of the catalyst support and the amount of the catalyst immobilized on these fragments is uneven in practical situations. The distribution of the amount of catalyst $M_{cat,i}$ in microelements referred by Eq. 26 is $10^{X/\beta}$, where X is the random number with normal distribution and the parameter β determines the broadness of the distribution (see Figure 19).

The results of morphogenesis simulations are illustrated in Figure 20 for the distribution P (with $\beta = 3$) and the more broad distribution Q (with $\beta = 2$) of catalyst activities $M_{cat,i}$ in the situations with and without ternary force interactions.

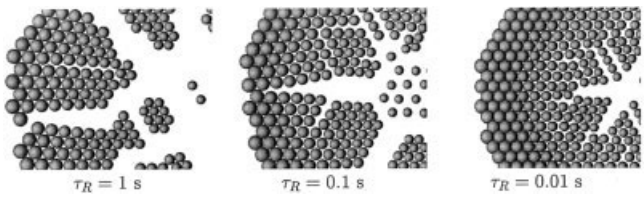

Figure 16. Morphology calculated with Maxwell interactions (detailed view of Figure 15 after 2 s of particle growth).

Qualitative effect of the relaxation time τ_R on the porosity of the resulting particle. Values of simulation parameters are the same as in Figure 15.

Figure 17. Effect of the monomer transport on the morphogenesis of the polyolefin particle.

Polymer yield $A_Y = 36$ $kg_{pol}/(g_{cat}$ h), Maxwell interactions, $\tau_R = 1$ s, maximum strain $e_{max} = 0.09$, bending modulus $G = 0.2E$, $\alpha_{max} = 5°$. The rectangle shows the relative spatial scale of the growing particle.

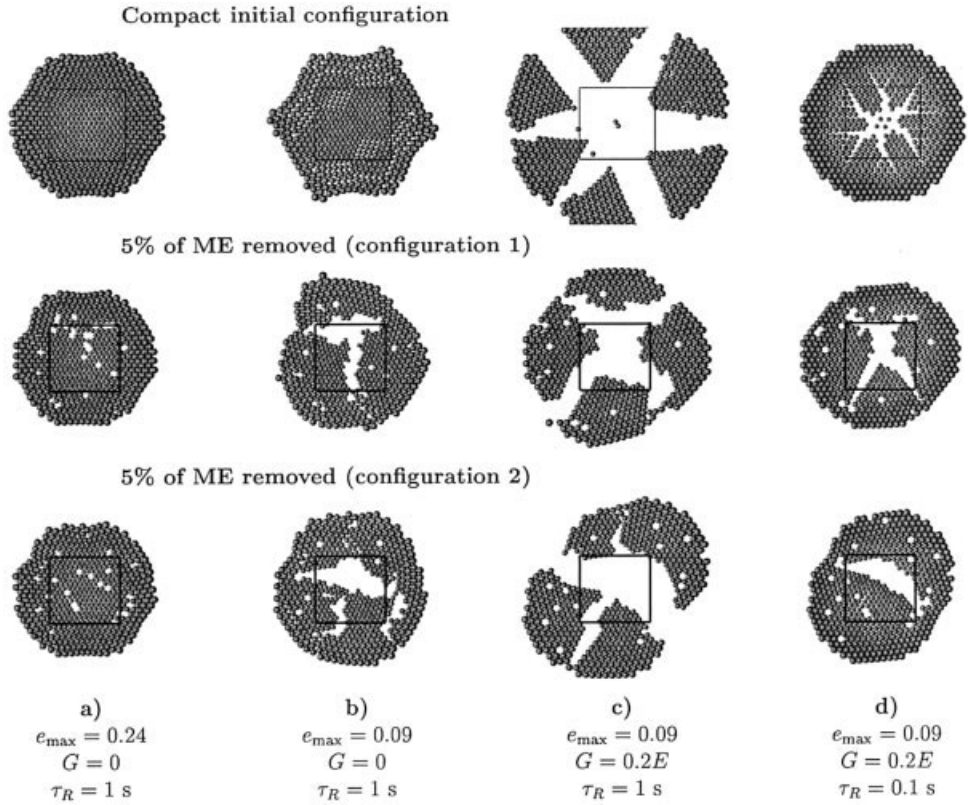

Figure 18. Effect of irregular initial conditions on the growth of polymer particles in the case of 5% removed microelements (ME).

Maxwell viscoelastic interactions. Polymer yield $A_Y = 36\ kg_{pol}/(g_{cat}\ h)$, $\Theta_0 = 5.6$. The rectangle shows the relative spatial scale of the growing particle.

When the ternary interactions are switched off, the content of macrocavities in the resulting particles is reduced and the particles are less porous than those simulated with ternary interactions. The case without ternary interactions can approximate a more plastic polymer at higher temperatures, where the microelements can more freely change the "bonding angles" with the other microelements. The porosity of the resulting particle increases with the broadening of the distribution of catalyst activity.

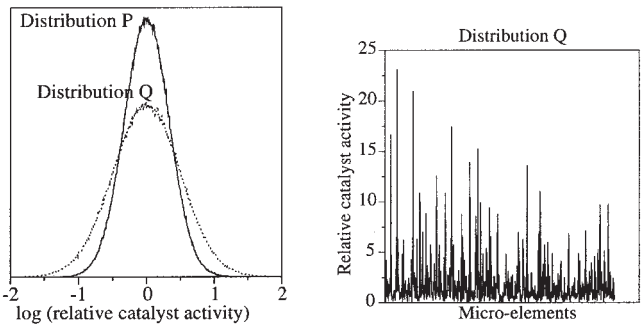

Figure 19. Log-normal distribution of catalyst activity $M_{cat,i}$ in microelements described as $10^{X/\beta}$, where X is the random number with normal distribution and the parameter β determines the broadness of the distribution.

In the distributions P and Q the parameter β has the value 3.0 and 2.0, respectively.

Examples of spatially 3-D evolutions of polymer particles are shown in Figure 21. The initial conditions were identical for all cases displayed in this figure. The presence of ternary interactions could even cause the particle disintegration into fines. No monomer transport limitations ($\Theta_0 = 0$) are considered in Figures 20 and 21. The distribution of catalyst activities in microelements is the consequence of the fragmentation of the catalyst particle and this distribution strongly influences the morphology of the polymer particle.

Evolution of particle porosity

The quantitative comparison of the porosity of the agglomerate of microelements with the experimental porosities of catalyst/polymer particles is hardly possible with the simple model used herein. Moreover, the evaluation of the average particle porosity in the model allowing overlaps of microelements is tedious. The more practical concept from the computational perspective is the concept of relative density of microelements ρ_μ calculated as the sum of volumes of 95% microelements closest to the center of gravity $\boldsymbol{x}_{COG}$ per volume of the sphere encapsulating 95% of microelements (see Figure 3). However, the concept of the density of microelements ρ_μ is well applicable only to particles with an almost spherical shape.

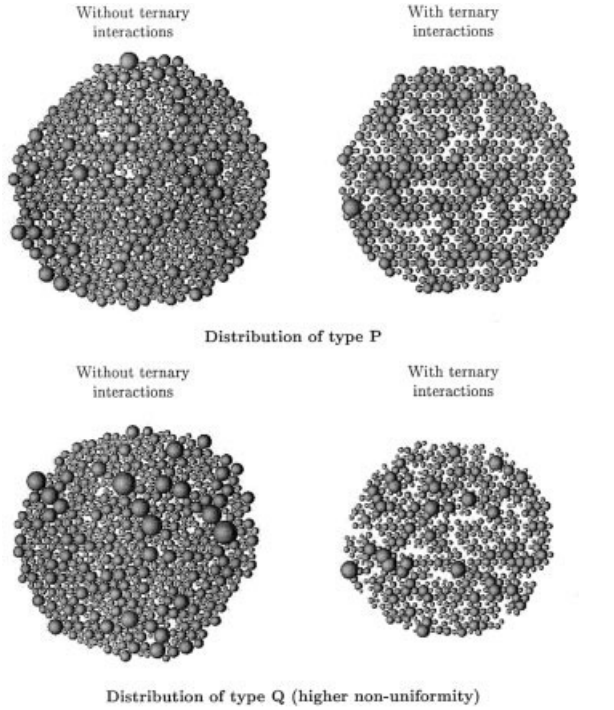

Figure 20. Effect of the nonuniform distribution of catalyst activity $M_{cat,i}$ on the morphogenesis of the particle.

Maxwell viscoelastic model. Polymer yield $A_Y = 10\ kg_{pol}/(g_{cat}\ h)$, relaxation time $\tau_R = 0.1$ s, maximum elongation $e_{max} = 0.04$, ternary interactions with bending modulus $G = E$, $\alpha_{max} = 5°$, $\Theta_0 = 0$. Situation at time $t = 50$ s.

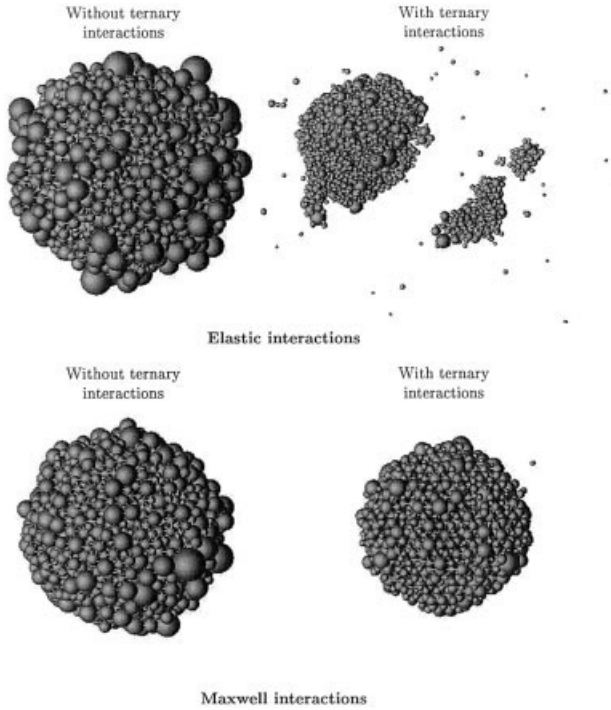

Figure 21. Effect of the nonuniform distribution of catalyst activity on the morphogenesis of the 3D particle.

Distribution of catalyst activity of the type Q. Polymer yield $A_Y = 10\ kg_{pol}/(g_{cat}\ h)$, relaxation time $\tau_R = 0.1$ s, maximum elongation $e_{max} = 0.04$, ternary interactions with the bending modulus $G = E$, $\alpha_{max} = 5°$, $\Theta_0 = 0$. Situation at time $t = 50$ s (left) and $t = 22$ s (right).

Figure 22 displays the evolution of the relative density of microelements ρ_μ for relaxation times $\tau_R \to \infty$ and $\tau_R = 1$, 0.1, and 0.01 s. The structure of these agglomerates is shown in Figure 15. The particles simulated with a lower value of τ_R (more plastic behavior) have a lower porosity compared to that of their elastic equivalents ($\tau_R \to \infty$). The evolution of ρ_μ in Figure 22 is nonmonotonous because of the definition of ρ_μ, which is scaled to volume encapsulating 95% of microelements. The formation of small cracks in the growing particle causes sudden fluctuations in ρ_μ.

So far we have discussed three important effects on the evolution of particle porosity: (1) nonuniform monomer concentration; (2) nonuniform distribution of catalyst activity in microelements; and (3) polymer properties represented, such as by the Maxwellian relaxation of stress. This paper considers the mass-transport resistance inside the growing particle to be relevant only in the early stages of particle growth. As the particle grows, the relative size of macrocavities and other imperfections of the internal morphology decreases (see Figure 15).

Let us now explore other possible driving forces causing the slow decrease of polymer particle porosity during its growth, as observed experimentally.[28,47] Although the neighboring microelements could interpenetrate in the case of the Maxwellian interactions, there has to be some driving force causing this interpenetration.

The temperature at the surface of the particle is lower than that in its center and this temperature difference causes spatial variations of the growth factor Γ, the elastic modulus E, and the relaxation time τ_R. However, the heat-transport resistance inside the growing particle is minimal[48] and cannot induce significant variations of the properties relevant to the evolution of particle porosity. Although the operation of industrial reactors

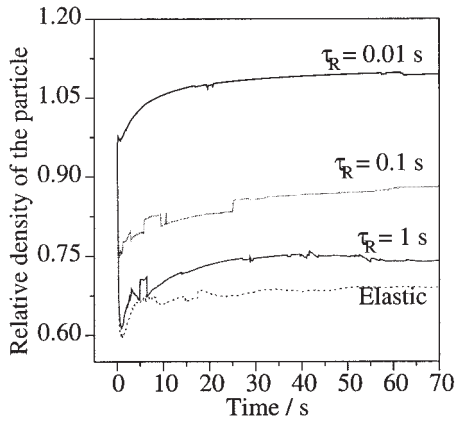

Figure 22. Dependency of the evolution of the relative density of microelements ρ_μ on the relaxation time τ_R of the Maxwell model.

The parameters are the same as in Figure 15.

is assumed to be isothermal, there are temperature differences occurring in the zones of the fluidized bed and the stirred-bed reactors. As the particle travels between these zones its temperature is dynamically varying and the timescale of temperature fluctuations can well interact, such as with the timescale of the stress relaxation. Therefore the effects of the nonstationary temperature field on particle porosity certainly deserves further study.

The inevitable presence of trace amounts of catalyst poisons in reactors can preferably deactivate the catalyst in the outer layers of the growing particle. In such a case the concentration of active catalyst sites in the particle center will be higher than that at the surface and the center of particle could thus grow faster. This effect could explain the fractured surface and compact core of particles observed by Nooijen.[49]

Another effect possibly contributing to the gradual decrease of particle porosity during its growth is the temporary accumulation of comonomer species in the center of the particle during the early stages of its growth caused by the convective flow into the particle.[12] Thus the content of the comonomer in the copolymer formed at the particle center is temporarily higher and the polymer in the center is thus "softer" than that formed at the particle surface.

Conclusions

The model of polyolefin particle represented by the agglomerate of microelements with mutual viscoelastic interactions acting among individual microelements has been developed. The model is capable of predicting industrially important cases of the formation of macrocavities, the hollow particles, the formation of fines, and the poor replication of the shape of the original catalyst particle. The preliminary concepts of this morphogenesis model were proposed in recent years.[8,9]

The morphogenesis model was intentionally kept simple. Therefore certain important effects, such as dynamics of the crystallization of the polymer phase, nonisothermal conditions in reactors, or a more realistic description of monomer transport in the evolving porous structure of the particle, were not taken into account. Some of these simplifications are addressed in the report of another study.[20] There is ample room for model improvement, especially in the section of viscoelastic properties of polyolefins and their stress–strain characteristics at reactor temperature. The characterization of mechanical behavior of polymer by the modulus, relaxation time, and maximum deformation used in this paper seems to be conceptually simple but is going to be replaced by characteristics routinely available from dynamic mechanical analysis and true stress–strain measurements.

In agreement with the effective-scale tension model[46] that describes the buildup and the relaxation of elastic tensions inside growing particles we have found that the mass-transfer resistance can lead to spatial variations in the expansion rate of polymer particle, which creates stress and can thus cause the occurrence of ruptures. This rupturing occurs early in the course of particle growth. In addition, our model is capable of predicting the shape and various types of the morphology patterns of the growing particle and is also capable of taking into account the nonuniform distribution of the catalyst inside the particle, which is at least as important for the particle evolution as the consideration of mass-transport resistances. The nonuniform distribution of catalyst activity results from the fragmentation of catalyst carrier. The control of catalyst fragmentation thus has a substantial effect on the final porosity of polymer particle. We have demonstrated that the same catalyst supported on different types of catalyst carriers (with different patterns of fragmentation) transforms to different porous structures of final polymer particles.

Various hypotheses and parameter combinations can be used to explain a single experimental observation such as the formation of hollow particles. The quantitative refinement of the proposed morphogenesis model is going to be a long process, with the goal of mapping from the architecture of catalyst particle and reactor conditions into the final morphology of polyolefin particles. The process of this refinement will certainly benefit from the expansion of the base of experimental observations, especially from the electron microscopy images of sections of particles. However, the morphogenesis model is capable of addressing, even without extensive refinement, the industrially relevant problems associated with particle morphology, such as the formation of fine particles and agglomerates in fluidized beds, the slow degassing of some grades of polyolefin powders, and so forth.

The developed model can be applied to a broad range of problems including the morphogenesis of impact polypropylene or other heterophase materials, the dynamics of the fragmentation of catalyst carriers in olefin polymerization, the foaming of polymers, and other situations. To our knowledge it is also one of the first attempts to describe the evolution of the spatially 3D structure of materials governed by the force interactions among the constituents of their structure. We believe that this type of the model—after the incorporation of additional parameters, such as electrostatic force fields—is capable of addressing the problems of colloid aggregation, sol–gel precipitation, and other diagenetic processes in mesostructured materials.

Acknowledgments

The support from the Czech Grant Agency (Projects 104/02/0325 and 104/03/H141) and from the Ministry of Education (MSM 6046137306) is gratefully acknowledged.

Notation

A_Y = polymer yield rate, $kg_{pol}/(g_{cat}\ h)$
A_{AB} = contact area between microelements, m^2
c_i = concentration of monomer in the ith microelement, mol/m^3
c_{bulk} = bulk concentration of the monomer, mol/m^3
c_{cat} = mass concentration of the catalyst, kg/m^3
C_i = dimensionless concentration
d_{ij} = distance of centers of microelements, m
D^{ef} = effective diffusivity, m^2/s
e = strain
e_{max} = maximum elongation
E = elastic modulus, Pa
E' = storage modulus, Pa
E'' = loss modulus, Pa
E_A = activation energy, J/mol
$\boldsymbol{F}_{ij}$ = binary interactions force, N
$\boldsymbol{F}_{ijk}$ = ternary interactions force, N
G = bending modulus, Pa
k = reaction rate constant, $m^3\ mol^{-1}\ s^{-1}$
k' = modified reaction rate constant, $m^3\ kg^{-1}\ s^{-1}$
k_0 = preexponential factor, $m^3\ mol^{-1}\ s^{-1}$
m_i = mass of the ith microelement, kg

$m_{cat,i}$ = mass of catalyst in the ith microelement, kg
$m_{cat,0}$ = characteristic mass of catalyst, kg
M_M = molecular weight of the monomer, kg/mol
$M_{cat,i}$ = dimensionless mass of catalyst
r_i = radius of the ith microelement, m
R_i = dimensionless radius
R = gas constant, J/(mol K)
R_{part} = characteristic radius of the particle, m
R_0 = characteristic length, m
s = radial coordinate, m
t = time, s
T = temperature, K
$\boldsymbol{u}$ = vector connecting microelements, m
u_0 = equilibrium distance between microelements, m
$\boldsymbol{v}_i$ = velocity of the ith microelement, m/s
V_i = volume of the ith microelement, m^3
$\boldsymbol{V}_i$ = dimensionless velocity
$\boldsymbol{x}_i$ = position vector of the ith microelement, m
$\boldsymbol{X}_i$ = dimensionless position
w_{cat} = initial weight fraction of the catalyst

Greek letters

α = value of the "bonding" angle, rad
α_0 = equilibrium value of the "bonding" angle, rad
α_{max} = limiting value of the "bonding" angle, rad
δ = phase lag of stress and strain, rad
η = viscosity, Pa·s
Γ = dimensionless growth factor
Ψ_E, Ψ_G = dimensionless elastic and bending moduli
$\Psi_{F_{ij}}$ = dimensionless force
ρ_i = density of the ith microelement, kg/m^3
σ = stress, Pa
τ = dimensionless time
τ_0 = characteristic time, s
τ_R = relaxation time, s
T_R = dimensionless relaxation time
Θ = Thiele modulus
ω = angular frequency, rad/s

Literature Cited

1. Floyd S, Heiskanen T, Taylor TW, Mann GE, Ray WH. Polymerization of olefins through heterogeneous catalysis. VI. Effect of particle heat and mass transfer on polymerization behavior and polymer properties. *J Appl Polym Sci*. 1987;33:1021-1065.
2. Llinas JR, Selo JL. *Method for Reducing Sheeting and Agglomerates during Olefin Polymerization*. WO Patent No. 01/66610; 2001.
3. Hafernick G, McNeil TJ, Prey TA, Tijerina JS. *Method for Reducing Sheeting during Olefin Polymerization*. WO Patent No. 99/02573; 1999.
4. Lee HK, Hunnisett CS, Hussein FD, Jacobsen LL, Painter RB. *Low Bed-Level Transition, Start-up, and Reactor Residence Time Control Using Sound Waves*. WO Patent No. 99/03901; 1999.
5. Debling JA, Ray WH. Morphological development of impact polypropylene produced in gas phase with a $TiCl_4/MgCl_2$ catalyst. *J Appl Polym Sci*. 2001;81:3085-3106.
6. Pelliconi A, Ciarrocchi A, Massari P. *Polypropylene Compositions Having Good Transparency and Improved Impact Resistance*. U.S. Patent No. 5 541 260; 1996.
7. Scheirs J, Bigger SW, Delatycki O. Structural morphology and compaction of nascent high-density polyethylene produced by supported catalysts. *J Mater Sci*. 1991;26:3171-3179.
8. Kosek J, Štěpánek F, Novák A, Grof Z, Marek M. Multi-scale modelling of growing polymer particles in heterogeneous catalytic reactors. In: Gani R, Jørgensen SB, eds. *Proceedings of the European Symposium on Computer Aided Process Engineering 11* (ESCAPE-11). Amsterdam: Elsevier; 2001:171-176.
9. Grof Z, Kosek J, Novák A, Marek M. Meso-scopic modeling of morphogenesis of polyolefin particles in heterogeneous catalytic reactors. In: Moritz HU, Reichert KH, eds. *Proceedings of the 7th International Workshop on Polymer Reaction Engineering*. DECHEMA and Wiley VCH; 2001;61-70.
10. Schmeal WR, Street JR. Polymerization in expanding catalyst particles. *AIChE J*. 1971;17:1189-1197.
11. Hutchinson RA, Chen CM, Ray WH. Polymerization of olefins through heterogeneous catalysis. X. Modeling of particle growth and morphology. *J Appl Polym Sci*. 1992;44:1389-1414.
12. Kosek J, Grof Z, Novák A, Štěpánek F, Marek M. Dynamics of particle growth and overheating in gas-phase polymerization reactors. *Chem Eng Sci*. 2001;56:3951-3977.
13. Adler PM, Thovert JF. Real porous media: Local geometry and macroscopic properties. *Appl Mech Rev*. 1998;51:537-585.
14. Grof Z, Kosek J, Marek M, Adler PM. Modeling of morphogenesis of polyolefin particles: Catalyst fragmentation. *AIChE J*. 2003;49:1002-1013.
15. Kakugo M, Sadatoshi H, Yokoyama M, Kojima K. Transmission electron microscopic observation of nascent polypropylene particles using a new staining method. *Macromolecules*. 1989;22:547-551.
16. Kittilsen P, Swendsen H, McKenna TF. Viscoelastic model for particle fragmentation in olefin polymerization. *AIChE J*. 2003;49:1495-1507.
17. Estenoz DA, Chiovetta MG. Olefin polymerization using supported metallocene catalysts: Process representation scheme and mathematical model. *J Appl Polym Sci*. 2001;81:285-311.
18. Pater JTM, Weickert G, Loos J, van Swaaij WPM. High precision prepolymerization of propylene at extremely low reaction rates—Kinetics and morphology. *Chem Eng Sci*. 2001;56:4107-4120.
19. Knoke S, Korber F, Fink G, Tesche B. Early stages of propylene bulk phase polymerization with supported metallocene catalysts. *Macromol Chem Phys*. 2003;204:607-617.
20. Grof Z, Kosek J, Marek M. Principles of the morphogenesis of polyolefin particles. *Ind. Eng. Chem. Res.* 2005;44:2389-2404.
21. Kakugo M, Sadatoshi H, Sakai J, Yokoyama M. Growth of polypropylene particles in heterogeneous Ziegler–Natta polymerization. *Macromolecules*. 1989;22:3172-3177.
22. Conner WC, Webb SW, Spanne P, Jones KW. Use of X-ray microscopy and synchrotron microtomography to characterize polyethylene polymerization particles. *Macromolecules*. 1990;23:4742-4747.
23. Kim I, Woo SI. Morphological study of HDPE prepared with the highly active silica supported $TiCl_4/MgCl_2$ catalyst. *Polym J*. 1989;21:697-707.
24. Weist EL, Ali AH, Naik BG, Conner WM. Morphological study of supported chromium polymerization catalysts. 2. Initial stages of polymerization. *Macromolecules*. 1989;22:3244-3250.
25. Han-Adebekun GC, Hamba M, Ray WH. Kinetic study of gas phase olefin polymerization with a $TiCl_4/MgCl_2$ catalyst. I. Effect of polymerization conditions. *J Polym Sci Part A: Polym Chem*. 1997;35:2063-2074.
26. Niegisch WD, Crisafulli ST, Nagel TS, Wagner BE. Characterization techniques for the study of silica fragmentation in the early stages of ethylene polymerization. *Macromolecules*. 1992;25:3910-3916.
27. Galli P, Collina G, Sgarzi P, Baruzzi G, Marchetti E. Combining Ziegler–Natta and metallocene catalysis: New heterophasic propylene copolymers from the novel multicatalyst reactor granule technology. *J Appl Polym Sci*. 1997;66:1831-1837.
28. Simonazzi T, Cecchin G, Mazzullo S. An outlook on progress in polypropylene-based polymer technology. *Prog Polym Sci*. 1991;16:303-329.
29. Costa MAS, Coutinho FMB, Maria LCS. The influence of some synthesis parameters on Ziegler–Natta catalyst performance. *Polym Bull*. 1993;31:249-254.
30. Pater JTM, Weickert G, van Swaaij WPM. Polymerization of liquid propylene with a fourth-generation Ziegler–Natta catalyst: Influence of temperature, hydrogen, monomer concentration, and prepolymerization method on powder morphology. *J Appl Polym Sci*. 2003;87:1421-1435.
31. Czaja K, Król B. Two-step polymerization of propylene over $MgCl_2$-supported titanium catalyst. *Macromol Chem Phys*. 1998;199:451-455.
32. Kittilsen P, McKenna TF. Study of the kinetics, mass transfer, and particle morphology in the production of high-impact polypropylene. *J Appl Polym Sci*. 2001;82:1047-1060.
33. Hoel EL, Cozewith C, Byrne GD. Effect of diffusion on heterogeneous ethylene-propylene copolymerization. *AIChE J*. 1994;40:1669-1684.
34. Naik SD, Ray WH. Particle morphology for polyolefins synthesized with supported metallocene catalysts. *J Appl Polym Sci*. 2001;79:2565-2579.
35. McKenna TF, Soares JBP. Single particle modelling for olefin poly-

merization on supported catalysts: A review and proposal for future developments. *Chem Eng Sci*. 2001;56:3931-3949.
36. Debling JA, Ray WH. Heat and mass transfer effects in multistage polymerization processes: Impact polypropylene. *Ind Eng Chem Res*. 1995;34:3466-3480.
37. Hamba M, Han-Adebekun GC, Ray WH. Kinetic study of gas phase olefin polymerization with a $TiCl_4/MgCl_2$ catalyst. II. Kinetic parameter estimation and model building. *J Polym Sci Part A: Polym Chem*. 1997;35:2075-2096.
38. Tsuji Y, Tanaka T, Ishida T. Lagrangian numerical simulation of plug flow of cohesionless particles in a horizontal pipe. *Powder Technol*. 1992;71:239-250.
39. Tsuji Y, Kawaguchi T, Tanaka T. Discrete particle simulation of two-dimensional fluidized bed. *Powder Technol*. 1993;77:79-87.
40. Mikami T, Kamiya H, Horio M. Numerical simulation of cohesive powder behavior in a fluidized bed. *Chem Eng Sci*. 1998;53:1927-1940.
41. Drozdov AD, Christianses JdeC. The effect of annealing on the elastoplastic and viscoelastic responses of isotactic polypropylene. *Comput Mater Sci*. 2003;27:403-422.
42. Young RJ, Lovell PA. *Introduction to Polymers*. 2nd Edition. London: Chapman & Hall; 1995.
43. Dutta NK, Edward GH. Generic relaxation spectra of solid polymers. I. Development of spectral distribution model and its application to stress relaxation of polypropylene. *J Appl Polym Sci*. 1997;66:1101-1115.
44. Brooks NWJ, Duckett RA, Ward IM. Temperature and strain-rate dependence of yield stress of polyethylene. *J Polym Sci Part B: Polym Phys*. 1998;36:2177-2189.
45. Brooks NWJ, Duckett RA, Ward IM. Effect of crystallinity and stress state on the yield strain of polyethylene. *Polymer*. 1999;40:7367-7372.
46. Kittilsen P, McKenna TF, Svendsen H, Jakobsen HA, Fredriksen SB. The interaction between mass transfer effects and morphology in heterogeneous olefin polymerization. *Chem Eng Sci*. 2001;56:4015-4028.
47. Bukatov GD, Zaikovskii VI, Zakharov VA, Kryukova GN, Fenelonov VB, Zagrafskaya RV. The morphology of polypropylene granules and its link with the titanium trichloride texture. *Polym Sci USSR*. 1982;24:599-608.
48. Floyd S, Choi KY, Taylor TW, Ray WH. Polymerization of olefins through heterogeneous catalysis. III. Polymer particle modeling with an analysis of intraparticle heat and mass transfer effects. *J Appl Polym Sci*. 1986;32:2935-2960.
49. Nooijen GAH. On the importance of diffusion of cocatalyst molecules through heterogeneous Ziegler/Natta catalysts. *Eur Polym J*. 1994;30:11-15.

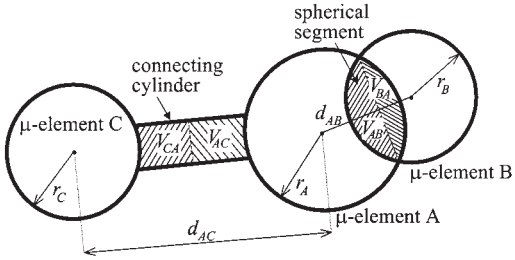

Figure A1. Illustration of the conservation of the volume of microelements.

Appendix: Conservation of the Volume of Microelements

The Eq. 2 system is strictly valid only in the case of spherical microelements that do not interpenetrate with their neighbors. Let us consider a general case, where the force interactions cause the microelements to interpenetrate or stretch apart. In this case we formulate the requirement of the conservation of the volume of microelements (see Figure A1). Let us denote the volume of the *i*th microelement subtracted as a result of the interaction with the *j*th microelement as V_{ji}. Then Eq. 3 could be reformulated for the case of the constant microelement density ρ_i as

$$\frac{dm_i}{dt} = \rho_i \frac{d\left(\frac{4}{3}\pi r_i^3 - \sum_j V_{ji}\right)}{dt} = k m_{\mathrm{cat},i} c_i \qquad \text{(A1)}$$

where the summation index j is taken over all microelements connected with the *i*th microelement. The volume V_{ji} is either a spherical segment in the case of overlapping microelements or it is a cylinder of arbitrary selected radius $(1/8)(r_i + r_j)$ for stretched microelements, that is

$$V_{ji} = \begin{cases} \frac{1}{3}\pi\left[\frac{r_j^2 - (d_{ij} - r_i)^2}{2d_{ij}}\right]^2\left[3r_i - \frac{r_j^2 - (d_{ij} - r_i)^2}{2d_{ij}}\right] & : \quad r_i + r_j \geq d_{ij} \\ -\pi\left(\frac{r_i + r_j}{8}\right)^2 \frac{d_{ij} - (r_i + r_j)}{2} & : \quad r_i + r_j < d_{ij} \end{cases} \qquad \text{(A2)}$$

Here d_{ij} is the distance of centers of the *i*th and the *j*th microelements. If two microelements interpenetrate, their diameters increase to conserve the total volume of microelements and they analogously decrease when the microelements are stretched apart. The assumption of the conserved volume of microelements is equivalent to Poisson ratio $\nu = 0.5$ used in the description of elastic behavior of incompressible materials. Polyolefins have a Poisson ratio ν close to this incompressible limit.

Certain locations could belong to the effective radius of more than two intersecting microelements. Such a situation, however, is not treated by our model. The introduction of the conservation of microelement volume by Eq. A1 causes the left-hand side of this equation to contain not only the term dr_i/dt, but also the term dr_j/dt. Thus this equation renders the system of ordinary differential Eqs. 1 and A1 semiexplicit.

All results displayed herein were obtained with the translational movement of microelements described by Eq. 1 and the growth of microelements described by Eq. 3 or their dimensionless analogs, that is, with a model that does not conserve the volume of the polymer phase because the microelements are allowed to overlap. We have found that neglecting the interpenetration of pairs of microelements causes only relatively slight "loss of the conserved volume." If the equations

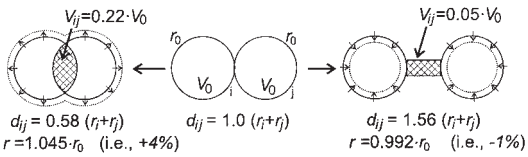

Figure A2. Quantitative effect of the interpenetration and the pulling away of two microelements on the conservation of the volume.

conserving the volume of microelements (Eqs. A1 and A2) were used instead of trivial Eqs. 2 and 3 then only minor changes in the results of simulations were observed.

For example, if two microelements with the radius $r_i = r_j = 1$ become interpenetrated and the distance between their centers is $0.58(r_i + r_j)$ then the overlapping volume is about 22% of the volume of one microelement (see Figure A2). According to Eqs. A1 and A2 the effective radii of both microelements have to increase about 4% to compensate for the "loss of the volume" caused by the interpenetration. In the case where two microelements are pulled apart the decrease of their effective radii is even smaller (-1%), as can be seen in Figure A2.

Manuscript received May 19, 2004, revision received Aug. 27, 2004, and final revision received Mar. 24, 2005.